



Investigating the representation of heatwaves from an ensemble of km-scale regional climate simulations within CORDEX-FPS convection

L. Sangelantoni^{1,2} · S. Sobolowski³ · T. Lorenz³ · Ø. Hodnebrog⁴ · R. M. Cardoso⁵ · P. M. M. Soares⁵ · R. Ferretti² · A. Lavín-Gullón⁶ · J. Fernandez⁶ · K. Goergen^{7,8} · J. Milovac⁶ · E. Katragkou⁹ · S. Kartsios⁹ · E. Coppola¹⁰ · E. Pichelli¹⁰ · M. Adinolfi¹¹ · P. Mercogliano¹¹ · S. Berthou¹² · H. de Vries¹³ · A. Dobler¹⁴ · D. Belušić^{15,20} · H. Feldmann¹⁶ · M. H. Tölle^{17,18} · S. Bastin¹⁹

Received: 26 February 2022 / Accepted: 21 March 2023 / Published online: 8 April 2023
© The Author(s) 2023

Abstract

Heatwaves (HWs) are high-impact phenomena stressing both societies and ecosystems. Their intensity and frequency are expected to increase in a warmer climate over many regions of the world. While these impacts can be wide-ranging, they are potentially influenced by local to regional features such as topography, land cover, and urbanization. Here, we leverage recent advances in the very high-resolution modelling required to elucidate the impacts of heatwaves at these fine scales. Further, we aim to understand how the new generation of km-scale regional climate models (RCMs) modulates the representation of heatwaves over a well-known climate change hot spot. We analyze an ensemble of 15 convection-permitting regional climate model (CPRCM, ~2–4 km grid spacing) simulations and their driving, convection-parameterized regional climate model (RCM, ~12–15 km grid spacing) simulations from the CORDEX Flagship Pilot Study on Convection. The focus is on the evaluation experiments (2000–2009) and three subdomains with a range of climatic characteristics. During HWs, and generally in the summer season, CPRCMs exhibit warmer and drier conditions than their driving RCMs. Higher maximum temperatures arise due to an altered heat flux partitioning, with daily peaks up to ~150 W/m² larger latent heat in RCMs compared to the CPRCMs. This is driven by a 5–25% lower soil moisture content in the CPRCMs, which is in turn related to longer dry spell length (up to double). It is challenging to ascertain whether these differences represent an improvement. However, a point-scale distribution-based maximum temperature evaluation, suggests that this CPRCMs warmer/drier tendency is likely more realistic compared to the RCMs, with ~70% of reference sites indicating an added value compared to the driving RCMs, increasing to 95% when only the distribution right tail is considered. Conversely, a CPRCMs slight detrimental effect is found according to the upscaled grid-to-grid approach over flat areas. Certainly, CPRCMs enhance dry conditions, with knock-on implications for summer season temperature overestimation. Whether this improved physical representation of HWs also has implications for future changes is under investigation.

Keywords Regional climate models · Multi-model ensemble simulations · Convection-permitting scale · Heatwaves

1 Introduction

Heatwaves (HWs) represent a particular category of weather extremes defined by persistently anomalous high temperatures (Perkins and Alexander 2013). Often studied from a climatological perspective, the governing spatial

and temporal scales place HWs as meteorological extreme events. These phenomena may have devastating impacts on nature and society, causing both a sharp mortality rate increase and limiting ecosystem functioning and services.

During recent decades, Central Europe and in general mid-latitudes, witnessed HWs with unprecedented severe impacts (Black et al. 2004; Miralles et al. 2014). Observed trends indicate a region-specific increase in the frequency and magnitude of HWs (Fischer and Schär 2010). Though it is complicated to attribute a cause-effect relationship between anthropogenic climate change and a specific event,

✉ L. Sangelantoni
lorenzo.sangelantoni@aquila.infn.it

Extended author information available on the last page of the article

several studies point out how a warmer background climate state increases the likelihood of high-intensity HW events (Fischer and Schär 2010; Seneviratne et al. 2012, 2021; Zscheischler et al. 2018).

HWs mainly rely on the atmospheric circulation component consisting of high-pressure synoptic systems advecting warm-to-hot air masses toward the affected region (Black et al. 2004; Feudale and Shukla 2007; Dole et al. 2011; Horton et al. 2015; Perkins 2015; Hong et al. 2018; Woollings et al. 2018; Kornhuber et al. 2019; Wehrli and Guillod 2019). The circulation component, in turn, modulates the degree of influence of other drivers, more importantly, but not only (e.g., vegetation feedback), soil moisture feedback. The latter is of particular importance in extreme events such as droughts and HWs and even manifests as a local source of predictability (Fischer et al. 2007; Hohenegger et al. 2009; Seneviratne et al. 2010; Taylor et al. 2013; Knist et al. 2017; Careto et al. 2018; Myhre et al. 2018; Soares et al. 2019; Zhou et al. 2019).

Soil moisture constrains the surface energy balance and the partitioning of latent and sensible heat fluxes, impacting air surface temperature, particularly in soil moisture-limited regions (Koster et al. 2004; Santanello et al. 2018). Land–atmosphere coupling can control HWs, amplifying intensity and persistence in the case of a combination of persistent blocking highs and dry soils, where the sensible heat is the dominant flux. A typical situation is represented by the well-documented 2003 HW over central and Western Europe. In this event, particularly dry conditions triggered a positive feedback between soil moisture and temperature extremes which exacerbated the HW intensity by about 40% with a secondary impact on the resulting synoptic circulation (Fischer et al. 2007; Miralles et al. 2014).

Regional Climate Models (RCMs) are a well-established tool to explore the interplay of HWs driving mechanisms, and their response to projected anthropogenic forcing (Molina et al. 2020; Vautard et al. 2013). RCMs bridge the gap between the coarse resolution projections from driving Global Climate Models (GCMs) and local climate information. In this regard, the latest generation of Convection Permitting RCMs (CPRCMs, < 4 km grid spacing) is considered a step change toward temporal/spatial resolution directly usable in regional-to-local scale climate impact studies (Kendon et al. 2012, 2020; Prein et al. 2013; Fosser et al. 2017; Prein et al. 2017; Berthou et al. 2018; Coppola et al. 2020; Adinolfi et al. 2021; Ban et al. 2021; Pichelli et al. 2021). Compared to previous RCM generations (Déqué et al. 2005; Giorgi et al. 2009; van der Linden and Mitchell 2009), km-scale modeling allows for an explicit treatment of relevant physical processes like deep convection without relying on parameterization schemes. Beyond the expected added value in short-duration precipitation extremes, km-scale modeling captures many small-scale mechanisms (e.g.,

hail, cloud processes, local-scale circulation patterns, coastal region dynamics, and tropical cyclones) underlying many high-impact phenomena, leading to more reliable projections, especially over complex orography (Kendon et al. 2020).

Another key aspect when moving to km-scale is the improved representation of land–atmosphere feedback (Knist et al. 2017, 2020; Jiang et al. 2019). In the present context, the feedback between soil moisture and precipitation is important for amplifying extreme events such as droughts and HWs. A relevant factor leading to the onset of a positive or a negative soil moisture precipitation feedback, is mesoscale circulations developing in response to horizontal gradients in surface heat fluxes ultimately driven by soil moisture spatial variability and orography (Findell and Eltahir 2003; Hohenegger et al. 2009; Cioni and Hohenegger 2017; Imamovic et al. 2017). In this regard, simulation-based studies demonstrate that a more realistic representation of the deep convection can present an essential advantage in reproducing soil moisture variability and consequent soil moisture precipitation feedback. (Hohenegger et al. 2009; Taylor et al. 2013; Hodnebrog et al. 2019; Sousa et al. 2020, Taylor et al. 2007). Differently, in parameterized-convection simulations, soil moisture precipitation feedback is dominated by grid column vertical exchange processes, generally combined to a rapid response to the increase of moist static energy over wet soils. This may overemphasize land–atmosphere interactions resulting in prevailing positive soil moisture precipitation feedback (Pielke 2001; Taylor et al. 2012, 2013).

Different soil moisture content between convection-parameterizing and convection-permitting simulations has a potential influence on temperature. For example, in the case of transition regions between wet and dry climates, considered regions of strong land–atmosphere coupling, a large part of temperature variability is driven by the soil moisture-temperature feedback (Koster et al. 2004, 2009; Miralles et al. 2012; Yang et al. 2018). When radiative fluxes increase and soil moisture decreases over time, flux partitioning changes in favor of the sensible heat flux, fostering anomalous high surface temperatures (Miralles et al. 2012, 2019).

In this study, we present the first ensemble-based investigation on the modulation of HWs and related processes when moving from a convection-parameterizing to a convection-permitting scale (km-scale). We take advantage of a multi-model ensemble of decade-long climate evaluation simulations at convection-permitting scale and the corresponding driving convection-parameterized RCMs from the CORDEX-FPS Convection initiative (Coppola et al. 2020; Ban et al. 2021; Pichelli et al. 2021). We analyze the modulation introduced by km-scale modeling over three subdomains of the greater Alpine region with specific topographic and climatic features, following five analysis steps: first a

description of the main HWs characteristics, temperature, timing, and persistence; followed by a cause and effect analysis on the surface energy balance; soil moisture; and summer season dry spell length. Finally, we explore the temporal evolution of forcing variables during HW and non-HW conditions.

In Sect. 2.1 the ensemble simulations and reference products considered are presented. In Sect. 2.2 the experimental setup is described. Results follow in Sect. 3. A discussion with a summary of the main findings and future research perspectives is presented in Sect. 4.

2 Data and experimental design

2.1 Model simulations

In this study, we analyze an ensemble of 15 CPRCMs simulations representing a subset of the evaluation simulations (covering the 2000–2009 period) performed within the CORDEX Convection Flagship Pilot Study (Coppola et al. 2020). These simulations consist of high-resolution

convection-permitting simulations (2–4 km grid-spacing) performed with 5 different RCMs (Table 1). Except for simulations run by UK Met Office (MOHC) and Justus-Liebig-University Giessen (JLU), all the CPRCMs are driven by the corresponding RCMs at an intermediate resolution (~12–15 km grid-spacing). Although the MOHC group is not using the intermediate step, they are providing the data from the UM model at the resolution of 12 km used for comparison in Berthou et al. (2020).

The multi-model ensemble setup includes a multi-physics ensemble using WRF with a perturbation of cloud microphysics, shallow convection, planetary boundary layer, and land surface model parameterizations. Moreover, sensitivity to nesting strategies is explored in the COSMO consortium, with all three members sharing the same numerical configuration but where: JLU directly downscales ERA-Interim; KIT and CMCC CPRCMs are driven by a 0.22° and 0.11° resolution RCM respectively. CMCC also adopts the urban scheme TERRA-URB (Wouters et al. 2016) for the CPRCM, accounting for the urban heat with expected impact on temperature modulation,

Table 1 List of ERA-Interim driven simulations from the different institutions and models used in this study

Institution		CPRCM	Resolution (km)	Driving RCM (domain) ^a	Resolution (km)
BCCR	The Bjerknes Centre for Climate Research (Norway)	WRF381BF	3	WRF (EURO-CORDEX)	15
CICERO	Center for International Climate and Environmental Research (Norway)	WRF381BJ	3	WRF (EURO-CORDEX)	15
IDL	Instituto Dom Luiz (Portugal)	WRF381BH	3	WRF (EURO-CORDEX)	15
UCAN	Universidad de Cantabria (Spain)	WRF381BI	3	WRF (EURO-CORDEX)	15
FZJ	Research Centre Jülich (Germany)	WRF381BB	3	WRF (EURO-CORDEX)	15
UHOH	University of Hohenheim (Germany)	WRF381BD	3	WRF (EURO-CORDEX)	15
AUTH	Aristotle University of Thessaloniki (Greece)	WRF381BG	3	WRF (EURO-CORDEX)	15
IPSL	Institut Pierre-Simon-Laplace (France)	WRF381BE	3	WRF/(EURO-CORDEX)	15
ICTP	International Centre for Theoretical Physics (Italy)	RegCM4	3	RegCM4 (Europe)	12
MOHC	Met Office Hadley Centre Exeter (UK)	UM	2.2	No ^b	No
KNMI	Royal Netherlands Meteorological	HCLIM38-AROME	2.5	RACMO (Europe)	15
HCLIM	HARMONIE-Climate community Danish Meteorological Institute (Denmark), MET Norway and Swedish Meteorological (Norway), Hydrological Institute (Sweden)	HCLIM38-ALADIN	3	ALADIN (Alps)	12
CMCC	Centro Euro-Mediterraneo sui Cambiamenti Climatici (Italy)	COSMO-CLM	3	COSMO-CLM (EURO-CORDEX)	12
KIT	Karlsruhe Institute of Technology (Germany)	COSMO-CLM	3	COSMO-CLM (Europe)	25
JLU	Justus-Liebig-University Giessen (Germany)	COSMO-CLM	3	No ^c	

^aNote that many groups are using European domain as an intermediate step. However, this domain is not necessarily the same between the groups, except for the EURO-CORDEX domain

^bAlthough, UKMO group is not using the intermediate step, they are providing the data from the UM model at the resolution of 12 km. This data was also used for comparison in the work of Berthou et al. (2018)

^cJLU has no RCM counterpart since performing a direct downscaling from ERA-Interim

heat fluxes partitioning, radiation, and relative humidity, over urban and surrounding areas.

The main difference between the CPRCMs and driving RCMs lies in the deep convection parameterization used to treat deep convective processes in the RCMs. The latter provides driving fields and act as a reference for comparison to km-scale simulations. In this regard, it is noteworthy that, for HCLIM and KNMI simulations, the driving RCMs are different from the nested CPRCMs. In those cases, it is not possible to disentangle the signal generated by the km-scale from other factors (e.g., differences in numerical schemes and dynamical configuration) which could affect nested simulations as well. Convection-parametrized RCMs are in turn forced by ERA-Interim initial and boundary conditions (Dee et al. 2011) along the CORDEX-FPS Convection evaluation period 2000–2009. Details regarding different RCM configurations in terms of the main numerical schemes adopted and how multi-physics ensemble variability is generated within the individual modeling consortia can be found in the recent study by Ban et al. (2021).

To isolate the km-scale modulation over specific topographical contexts, three subdomains of the greater Alpine region are selected (Fig. 1). The first domain consists of some of the most complex topography of the Alpine region. The second domain presents opposite features, consisting of a totally flat-terrain portion of the Po valley. The third domain, the Adriatic region, has multifaceted orography, and a large portion is represented by coastal areas. In this latter subdomain is applied a land-sea mask which filters out sea grid nodes.

2.2 Reference datasets

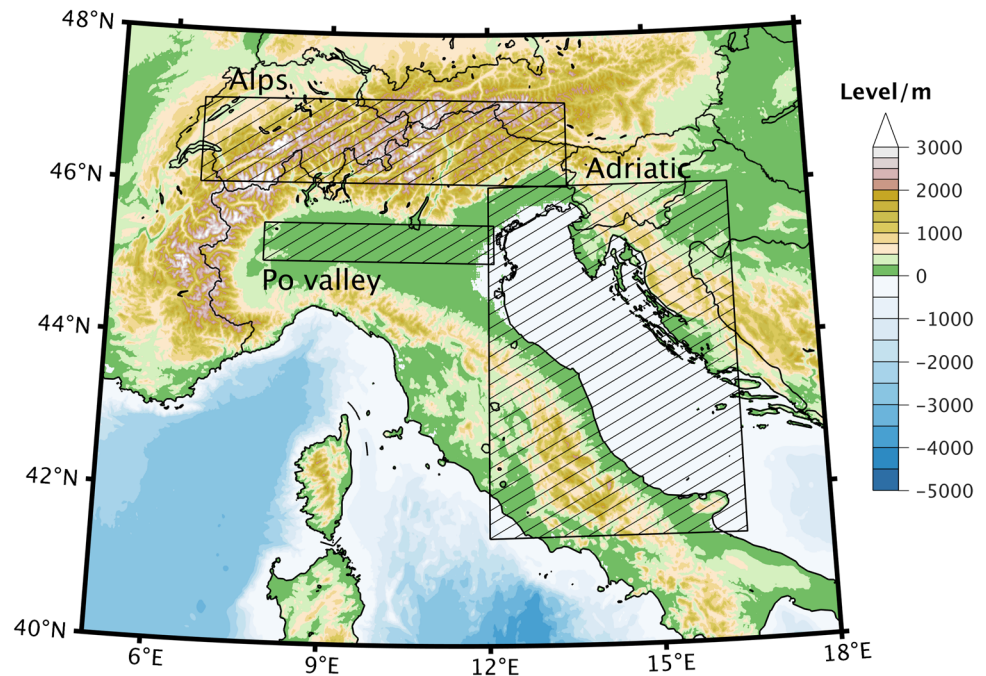
We use several reanalysis and observation-based reference products. For the daily maximum temperature these are:

- UERRA HARMONIE-MESCAN SURFACE which combines UERRA HARMONIE reanalysis (Bazile et al. 2017) with a spatial resolution of 11 km over entire Europe driven by ERA-Interim, to a surface analysis system, MESCAN SURFACE (Ridal et al. 2017) producing surface analysis over Europe with a spatial resolution of 5.5 km available over the period 1961–2018
- ERA5-Land (Muñoz-Sabater et al. 2021), the European Centre for Medium-Range Weather Forecasts (ECMWF) enhanced global dataset for land component and surface variables of ERA5 reanalysis (9 km resolution, 1981 to present).
- The gridded EOBS 23.0e dataset (Haylock et al. 2008) at ~11 km resolution over Europe (available from 1950-01-01 to 2020-06-30).
- Underlying local-scale measurement stations datasets ECA&D V24 (Klein Tank et al. 2002) provided by the European Climate Assessment & Dataset observational stations (<http://www.ecad.eu>).

For the soil moisture:

- ESSMRA reanalysis (Naz et al. 2020) consisting of 16 years (2000–2015) daily high-resolution surface soil moisture dataset (3 km resolution) over Europe based

Fig. 1 Geographical domain considered in this study. The three black boxes indicate subdomains (Alpine region, Po valley, and Adriatic region) analyzed in more detail



on coarse-resolution satellite-derived soil moisture data assimilated into the community land model (CLM3.5).

- ERA5-Land (see above).

For the precipitation:

- EURO4M-APGD (Isotta et al. 2014) daily precipitation gridded dataset (5 km resolution) over the Alpine region, available for the 1971–2008 period (here considered for the 2000–2008 period).
- GRIPHO (Fantini 2019) hourly gridded precipitation dataset over Italy based on surface station observations (3 km resolution) covering 2001–2016 period (here considered for the 2001–2009 period).

2.3 Analyses

Scientific literature reports a broad number of HW definitions and measures (Perkins and Alexander 2013). A general framework tends to identify at least three days in a row exceeding a certain percentile-based threshold (Perkins et al. 2012; Russo et al. 2015) allowing for a comparison of HW events on different climate types. In this study, we define an HW event as a hot-day spell lasting for at least five days, similar to Fischer and Schär (2010) and Vautard et al. (2013).

A hot day is here defined as a day with a maximum temperature (Tmax) equal to or larger than the 90th percentile of the summer season (June, July, and August months, JJA) statistical distribution of the 2000–2009 period which defines the temporal domain of the present study. Within the evaluation experiment period, we focus on three major HW events (2003, 2006, and 2007). Their general features and atmospheric circulation anomaly patterns are shown in the supplementary materials Fig. SM1, based on ERA5 reanalysis.

As already mentioned, HWs forcing can be mainly discerned in local-scale forcing and large-scale forcing (Hong et al. 2018). In this study, we only evaluate local-scale forcing, postulating that large-scale patterns are simulated similarly between CPRCMs and RCMs during HW events.

In this context, exploratory analyses performed on 500 hPa geopotential height and 850 hPa soil moisture divergence flux (shown in Figs. SM 2 and SM 3 respectively) do not disclose major differences in mesoscale circulation patterns during both HW and non-HW conditions in the two resolutions. Albeit mesoscale dynamics examination lays beyond the scope of the present study, it can be observed that RCMs are characterized by more pronounced orography-driven moisture convergence/divergence zones (especially in the 2003 HW), although in the face of similar moisture flux magnitude. Albeit taking into consideration only a single pressure level (see additional discussion in the

supplementary material following Fig. SM 3) this could suggest differences in relevant structural properties of PBL and precipitation triggering mechanisms like moisture advection and more intense updrafts.

The following analyses are performed.

(i) First analysis regards a temperature-based characterization of HWs represented by CPRCMs and RCMs. HWs magnitude, timing, and persistence at the two resolutions are shown. Then, statistical distribution properties of daily maximum and daily mean temperature at the two resolutions are assessed, considering only HWs and the whole summer season. These analyses, including the selection of HW events, consider spatial averages computed on native simulations grid resolution.

Then, we compare HWs mean Tmax produced by RCM and CPRCM ensembles and derive the corresponding bias considering EOBS dataset as a reference product. Finally, HW distribution-based magnitude index (HWMId, Russo et al. 2015) is derived for the RCM and CPRCM ensembles (Eq. 1).

$$M = \sum_{d=1}^n \frac{T_{\max}(d) - P25}{P75 - P25} \quad (1)$$

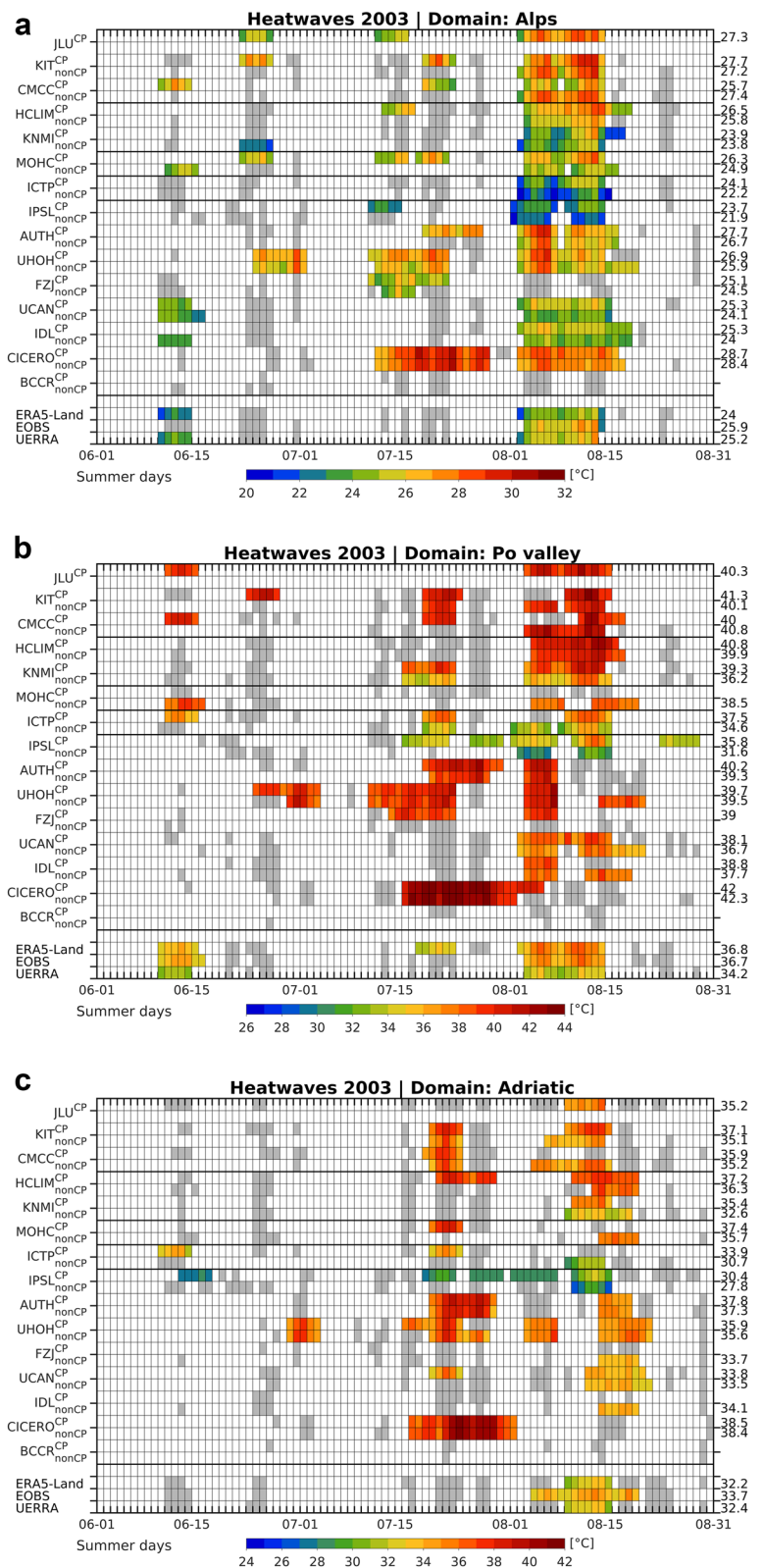
where Tmax(d) represents the Tmax of a HW day and n is the duration of the HW in days. The interquartile range (IQR) at the denominator is a measure of the variability of the (grid-node-specific) time series and composed by summer season daily Tmax in 2000–2009. In our case, differently from Russo et al. (2015), who derived the IQR of a 30-year period yearly Tmax, the IQR refers to the 2000–2009 JJA daily Tmax statistical distribution.

HW magnitude metric (HWMId), consists of a cumulative anomaly of Tmax during a given HW, quantifying how a HW has been anomalous in function of the corresponding statistical distribution properties. Results from all models are averaged to obtain the ensemble mean value. Concerning the unit, if the magnitude on HW day d is for example x, then the Tmax anomaly from the evaluation period 25th percentile is x times the IQR which represents the HW magnitude unit.

To characterize spatial patterns, in this latter set of analyses is followed a grid-node by grid-node approach over a domain encompassing the three subdomains previously described. To make results comparable, all CPRCMs are remapped into a common 3 km resolution grid and the same is done for the RCMs over a common 15 km grid.

When compared to the reference product, both the CPRCMs and RCMs are remapped into the ~ 11 km resolution EOBS grid. Here, the three HWs reported (2003, 2006, and 2007) have been selected considering temporal segments with the largest number of models and reference products reproducing a HW (2–14 Aug., 20–30 Jul., 15–25 Jul. respectively, see e.g., Fig. 2). However, this approach

Fig. 2 Spatially averaged HWs daily maximum temperature produced by RCM and CPRCM simulations and the reference products UERRA, EOBS, and ERA5-Land (left y-axis). The x-axis reports summer days. Gray-shaded cells indicate daily Tmax exceeding the evaluation period summer seasons' 90th percentile but not constituting an HW event. In the right y-axis are reported the mean of HWs Tmax. Results refer to the summer season of 2003 for the three subdomains: Alps (a), Po valley (b), and Adriatic (c)



presents the limitation of disregarding grid-node specific differences in terms of HWs occurrence and duration, that are a function of the grid node Tmax distribution properties.

Finally, we present a JJA Tmax station-scale evaluation to assess the potential added value of CPRCMs in comparison to their driving RCMs. This analysis relies on local-scale

ECA&D V24 dataset as a reference product. Only the measurement stations providing the highest quality code and with more than 90% of data available during the evaluation period 2000–2009 are selected. Observed time series are compared to the nearest neighborhood grid nodes of RCM and CPRCMs. Original resolutions are here considered, with no interpolation performed. The unique longitude-latitude couples, identifying the i th reference site common to the two resolutions are processed. Potential added value provided by higher resolution CPRCMs compared to the driving lower resolution RCMs is assessed through a Distribution-based Added Value (DAV, Soares and Cardoso (2018)) metric, derived at each reference site. This metric measures the common area between a simulated and an observed statistical distribution and is developed from a PDF skill score (S score) introduced by Perkins et al. (2007). For each observed and simulated time series frequency histograms are defined with bins width of 1 °C and encompassing all the observed values range. For the two resolutions the common area between observed and simulated distributions is computed, representing an integral of the curve defined by the minimum between observed and simulated frequencies of each distribution bin.

$$S_{rcm} = \sum_1^n \min(Z_{rcm}, Z_{obs})$$

$$S_{cprcm} = \sum_1^n \min(Z_{cprcm}, Z_{obs}) \quad (2)$$

where S is the integral of the correspondence between the simulated and observed frequencies (Z) and n is the number of distribution bins. Finally, the DAV value is derived as a percentage difference of the S value resulting from the two resolutions (S_{rcm} and S_{cprcm}).

$$DAV = \frac{S_{cprcm} - S_{rcm}}{S_{rcm}} * 100 \quad (3)$$

A second configuration of the DAV metric considers a grid node-by-grid node approach following Careto et al. (2022) where both simulated datasets (CPRCMs and RCMs) have been conservatively interpolated into the reference product EOBS (~ 10 km resolution). A constant lapse rate of -6.5 °C km $^{-1}$ is considered for the interpolation. Prior to the interpolation the orography effect is removed adiabatically adjusting temperature to the mean sea level. After the interpolation the temperature is adiabatically adjusted once again to the orography of the destination grid.

(ii) In a second analysis section, the focus is on the surface energy balance at the two resolutions during HW events. Spatially averaged hourly time series of heat fluxes produced by CPRCMs and RCMs during HW events are compared, and the modulation of HWs maximum temperature

as function of the Bowen ratio (ratio between sensible and latent heat fluxes) is assessed. Moreover, we assess spatial patterns of the mean evaporative fraction (evapfr) defined as the latent heat flux (hfls) divided by the sum of the latent and the sensible heat flux (hfss) to highlight differences in CPRCMs and RCMs land-atmosphere coupling strength. This metric is derived for the 2003 HW and for all the evaluation period summer seasons over an area including all the three subdomains considered. Here, all the RCMs remapped into a ~ 15 km resolution grid, and CPRCMs into a ~ 3 km resolution grid.

(iii) The third analysis section focuses on soil moisture during HW events, summer months and the entire annual cycle. Here, both spatially averaged time series and grid-node by grid-node spatial patterns are presented. As for the previous analyses, the latter consider all the RCMs remapped into a ~ 15 km resolution grid, and CPRCMs into a ~ 3 km resolution grid.

(iv) We explore the mean and different statistics of summer season dry spell length (DSL) as reproduced by CPRCMs and RCMs. This is considered a key factor driving soil moisture content differences between the two resolutions. Consistently to the previous analyses, RCMs and CPRCMs are respectively remapped into common resolution grids.

(v) Finally, we analyze the temporal evolution of a set of variables related to land surface (soil moisture and heat fluxes) and atmospheric state (precipitation and PBL height) to distinguish forcing during HW and non-HW conditions. This analysis considers two representative summer seasons and spatially averages for the Po valley subdomain.

3 Results

3.1 Temperature

Figure 2 shows an initial characterization of the intensity, timing, and persistence of HWs produced by CPRCMs, driving RCMs, and three reference products considering their own Tmax statistical distributions.

Results refer to the 2003 summer season and the three subdomains corresponding to the Alps, Po valley, and Adriatic regions, displayed in panels a, b, and c respectively. Results for the 2006 and 2007 summer seasons are shown in Fig. SM 4. Each panel consists of a daily-based comparison of spatially averaged Tmax at the two resolutions. The x-axis reports summer days (JJA months) whereas the left y-axis lists models at CP and non-CP resolution (JLU only provides CP runs). In the right y-axis are reported the mean of HWs Tmax. In case of multiple events, this value refers to the most intense event (i.e., the largest cumulative number of Celsius degrees above the 90th percentile). Results for

the reference products UERRA, EOBS, and ERA5-Land are reported in the bottom lines. Different panels show results for different HWs (rows) and domains (columns). Horizontal thick black lines distinguish different modeling consortia.

The HW of 2003 generally stands out for magnitude, persistence, and number of events. Over the Alps domain, CPRCMs and RCMs produce HWs Tmax close to the reference products' mean value or slightly higher. CICERO and KIT simulations stand out with mean HW Tmax warm biases up to ~ 4 °C. Over Po valley, regardless of the HW considered, both CPRCMs and RCMs show large hot biases up to 6–8 °C. The Adriatic region domain shows intermediate biases between the Alps and Po valley domains. However, the robustness of deviation between simulations and reference products is hindered by the large discrepancies among these latter, up to ~ 2.5 °C, especially over the Po valley.

It can be observed that CPRCMs and corresponding RCMs show similar timing and persistence for 2006 and 2007 events Fig. SM 4. Larger differences, up to cases where a short event is reproduced only in one of the two resolutions (e.g., MOHC Alps 2003), can be observed in the 2003 summer season and also in the 2006 HW over Po valley and Adriatic. For what concerns Tmax values, excluding KNMI (over the Alps) and CMCC runs (over the three domains), CPRCMs tend to produce higher values than the RCMs. Considering the mean of the HW Tmax, CPRCMs-RCMs differences are generally around 1.0 °C. However, in some cases like IPSL, ICTP, MOHC, and KNMI, differences over Po valley can exceed 3 °C in 2003 and 2006 HWs. These higher temperatures represent an improvement for IPSL and, although to a lesser extent, for the ICTP CPRCMs. Over Po valley, MOHC CPRCM's higher temperature signals a worsening compared to the RCM. It is peculiar the case of KNMI showing similar CPRCMs and RCMs mean Tmax over the Alps and CPRCM 3 °C warmer than the RCM over Po valley. Also in this case, this modulation leads to an increased warm bias over reference products. Within the WRF multi-physics ensemble, differences between CPRCMs and RCMs typically do not exceed 1 °C with UHOH RCM showing higher Tmax than the CPRCM in the 2006 event over the Po valley. In this context, as previously mentioned, IPSL CPRCM stands out with a larger warm modulation of the RCM signal over the Po valley and Adriatic regions. It is noteworthy that IPSL and UHOH WRF simulations share the same combination of physics schemes except for the microphysics scheme (i.e., Thompson and the aerosol-aware Thompson respectively).

Box plots in Fig. 3 summarize statistical properties of the spatially averaged HWs daily Tmax. In the upper panels, distributions are built on Tmax characterizing the most intense HW events for each of the three summer seasons. The bottom panels show daily Tmax distribution for the summer

months considering the whole evaluation period. According to the median of the ensembles (black dot within the boxes), CPRCMs Tmax is ~ 1 °C higher than the corresponding RCMs ensemble. However, relevant inter-model and intra-model (differences between CPRCMs and driving RCMs) spread can be observed. Firstly, considering the HWs box plots median differences about 6 °C results among different models. Regarding the intra-model differences, within the WRF ensemble, IDL and UCAN WRF show CPRCMs Tmax ~ 1.5 °C higher than the corresponding RCMs over the Alps and Adriatic domains. As previously mentioned, ICTP, MOHC, and KNMI (over the Po valley) show CPRCMs Tmax up to more than 3 °C higher than the RCMs.

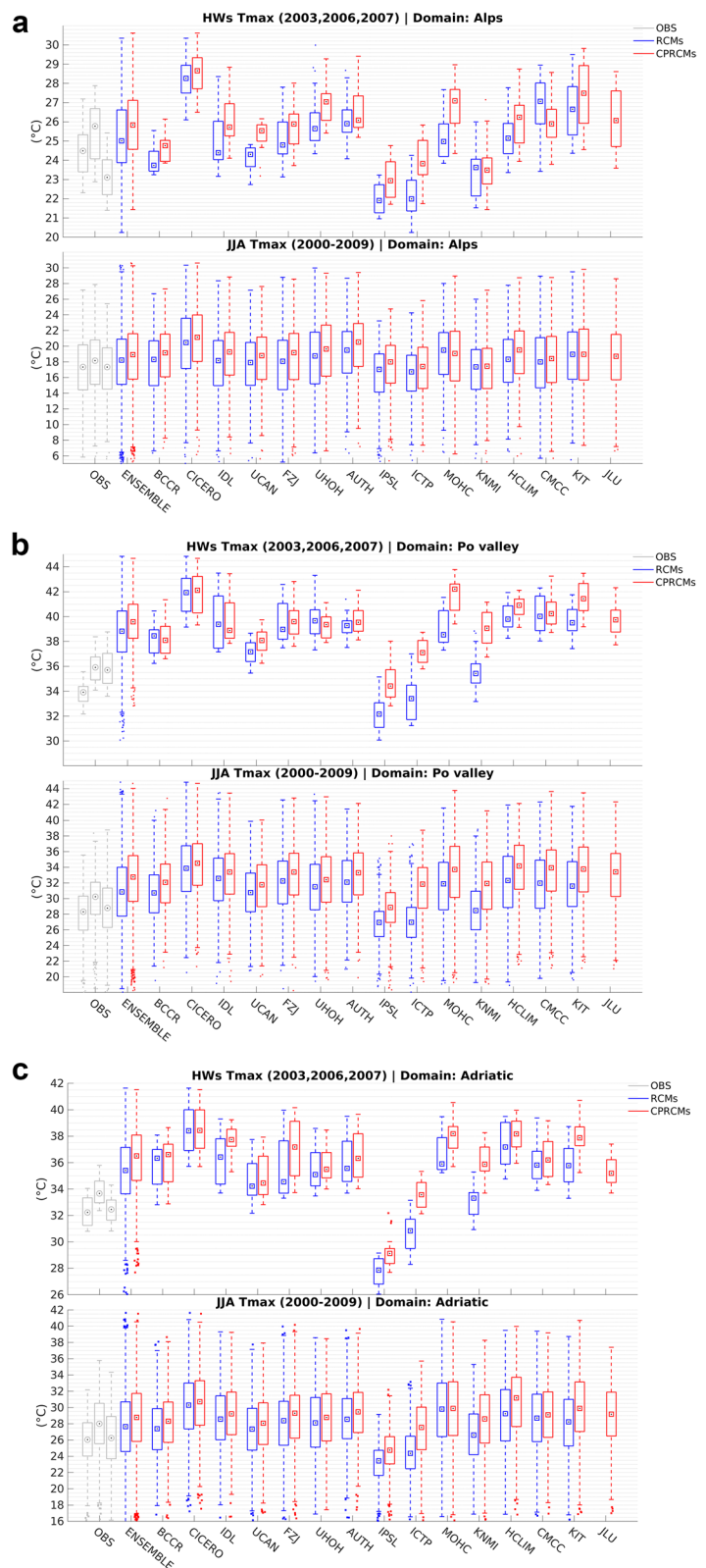
Within COSMO simulations a different tendency between CMCC and KIT results with the former showing higher Tmax in the RCM than the CPRCM over the Alps domain. Noteworthy are the differences between KIT and JLU with the latter generally closer to reference products. The two CPRCMs share the same numerical configuration but a different downscaling approach (a direct downscaling of ERA-Interim for the JLU). This aspect points out that downscaling strategy can modulate temperature extremes as well, representing a further level of uncertainty.

Over the whole evaluation period (bottom panels of Fig. 3), simulated and reference product distribution get much closer than when only HW days are considered. Also, a consistent reduction of differences among the reference datasets can be observed. However, it has to be noticed that, when considering the entire evaluation period, substantial differences among domains come up. Within the ALPs similar CPRCMs and RCMs Tmax are observed, while conversely, consistently higher CPRCMs Tmax compared to RCMs occur in the Po valley.

Differently from the other subdomains, over Po valley, also CMCC shows higher Tmax in the CPRCM. Considering the high concentration of Po valley urbanized areas, this could be regarded as the cumulative effect of the urban scheme adopted in the CPRCM. Here, the median of the CPRCMs ensemble is higher than the corresponding RCM ensemble by about 2 °C. It is noteworthy that IPSL, ICTP, MOHC, and KNMI CPRCMs run produce Tmax up to more than 3 °C higher than the driving RCMs, even when the entire evaluation period distribution is considered. The Adriatic region domain shows intermediate results between the Alps and Po valley domains.

A spatial patterns analysis over a domain encompassing the three subdomains is presented in Fig. 4. This consists of reference products and simulation ensemble means (panels a and b respectively) physical values, differences between RCM and CPRCM ensembles and EOBS (panels c), and RCM and CPRCM ensembles HWs magnitude metric as derived in Eq. 1 (panels d). Results for the representative 2003 HW are shown, whereas 2006 and 2007 results are

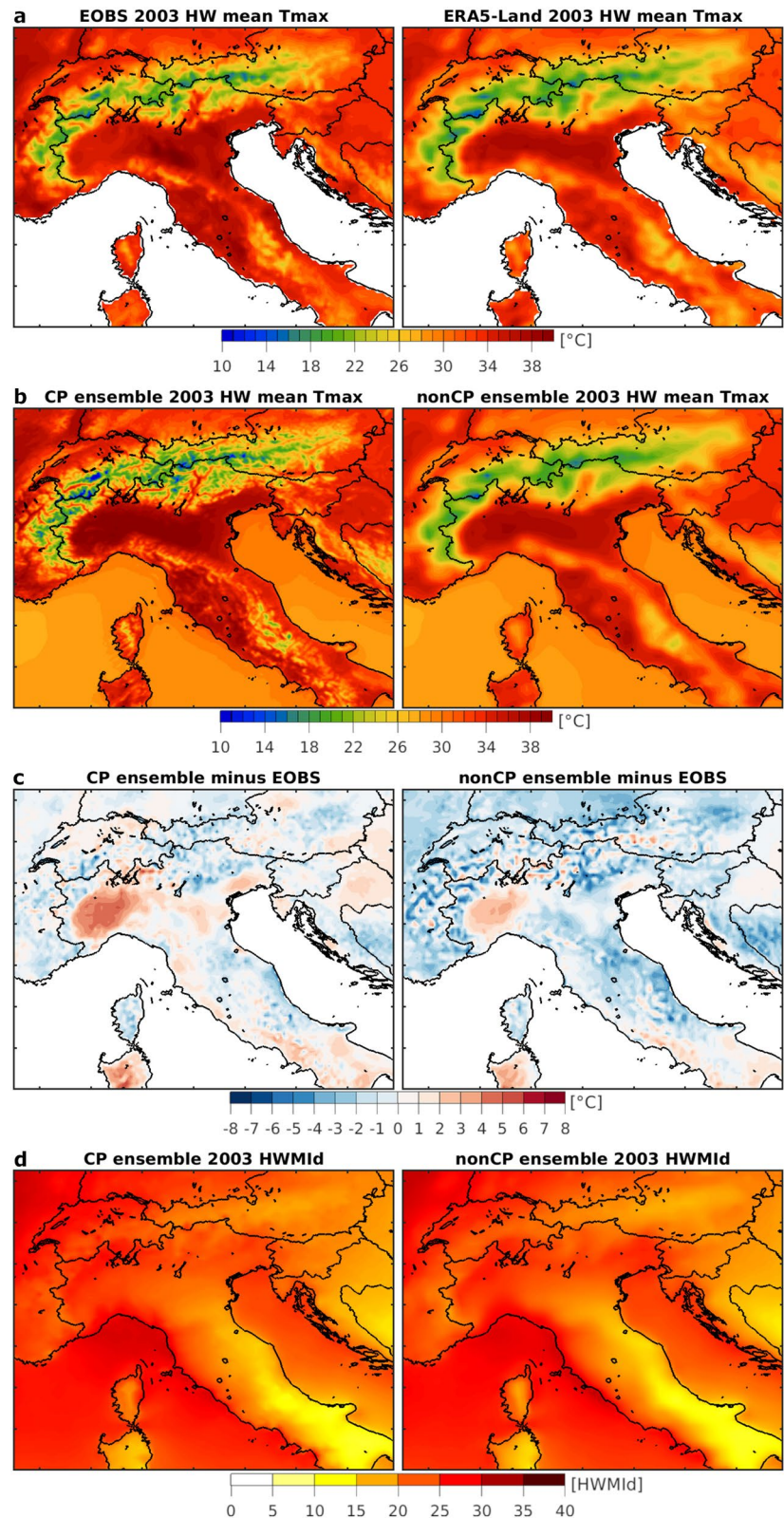
Fig. 3 Upper panels: box plots summarizing statistical distribution built on spatially averaged HWs Tmax for 2003, 2006, and 2007 summer seasons for the reference products (UERRA, EOBS, and ERA5-Land, gray boxplots from left to right) and models at the two resolutions. Bottom panels: same as upper ones, but with statistical distributions built on daily maximum temperature of the entire evaluation period (all summer seasons 2000–2009). Results are shown for the three subdomains: Alps (a), Po valley (b), and Adriatic (c). On each box, quartiles (central mark and box edges), extreme values within the 1.5 interquartile range from the box edges (whiskers) are represented



reported in Fig. SM 5. A comparison between the two reference products confirms how ERA5-Land produces lower Tmax than the EOBS dataset. Moving to simulations, the

CPRCMs ensemble generally shows higher temperatures than the nonCP ensemble mean, especially over flat terrain (up to ~2 °C). Higher CPRCMs ensemble Tmax translates

Fig. 4 Mean of the daily Tmax during the 2003 HW for the two reference products EOBS and ERA5-Land (**a**); for the CPRCMs and RCMs ensemble means (**b**). Differences between CPRCM and RCM ensemble means and EOBS mean HW Tmax (**c**). HWMId for the CPRCM and RCM ensemble means (**d**). This latter represents the average of the index results from each individual model



into a reduction of the generalized cold bias in the RCM ensemble, but also an error increase in regions with warm RCM biases, such as the upper Po valley. Considering 2006

HW, a warmer CPRCMs ensemble signals an increase in warm bias. This can be mainly observed again over the flat terrain of the Italian peninsula. Over the northern part of

the domain, RCMs ensemble cold bias shifts into a similar magnitude warm bias in the CPRCMs ensemble. Similar modulation patterns can be observed also in the 2007 event.

HW magnitude index shows, despite the higher CPRCMs ensemble Tmax, a similar cumulative anomaly, namely the HW has, in statistical terms, a similar location in the two resolution distributions. This feature, confirming the results of Fig. 4 (bottom panels), suggests a shift toward warmer values of the CPRCMs PDF instead of a shift limited to the distribution right tail. In Table 2 are reported mean HW metrics consisting of mean Tmax, HWMId, and persistence for the reference products, CPRCM, and RCM ensemble means. Values refer to the most intense HWs of the three summer seasons considered. Besides generally higher Tmax, CPRCMs are also characterized by lower inter-model spread over Po valley. As previously mentioned, mean HWMId and HWs persistence do not show substantial differences between the two resolutions.

We conclude with temperature-based analysis by presenting the results for a point-scale evaluation of JJA Tmax for each model and the corresponding ensemble mean. Results from 146 reference sites are shown. Considering original model grids this number can slightly vary across models as a function of the different resolutions and if the specific reference site is seen as a land or a sea node by the specific model grid. In Fig. 5a is considered the entire evaluation period summer season daily Tmax statistical distribution whereas in Fig. 5b the DAV is computed only considering

the distribution right tail (90th–99th percentiles). The ensemble consists of an average of all the model results for the specific reference site. Violin plots show a direct comparison of how well observations are captured by the two resolutions in terms of observed-simulated statistical distribution matching. Here if a model perfectly simulates the observed station conditions, the S skill score will equal one, which is the total sum of the frequency at each bin (when the entire statistical distribution is considered). An S skill score PDF is built simply considering S scores from all the reference stations. Maps in the upper right subplot show the geographical distribution of the reference sites and corresponding ensemble mean DAV values (Eq. 3). The percentage of reference sites characterized by $DAV > 0$, i.e. the CPRCM run adds value on the driving RCM, is indicated on the lower left corner of the panel. Considering the ensemble mean, 69% of reference sites present a $DAV > 0$ indicating an improved representation of the observed JJA Tmax performed by km-scale simulations. Larger positive DAV values can be found in areas of complex-topography alpine region sites and Croatian coastline sites. Analyzing results from individual ensemble members, largely different responses result. The positive DAV percentage varies from 25% for the HCLIM to 94% for the ICTP (not shown). In this regard, it is however essential taking into account, besides the mere CPRCM improvement measure, also the S score performed by the driving RCM. In fact, where large positive DAVs result (e.g. ICTP and IPSL) we can see poorer

Table 2 Reference products and simulated mean HW metrics. Values refer to most intense HW for each of the three summer seasons considered (2003, 2006, and 2007)

HW metric	Dataset	Domains		
		Alps	Po valley	Adriatic
Mean Tmax (°C)	UERRA	24.4	33.8	32.3
	EOBS	25.1	35.3	33.7
	ERA5-Land	23.1	34.8	32.4
	CPRCMs ensemble	25.7 (± 1.5)	39.4 (± 1.8)	36.0 (± 2.2)
	RCMs ensemble	24.8 (± 1.5)	38.0 (± 2.2)	34.6 (± 2.0)
HWMId	UERRA	14.0	17.5	12.2
	EOBS	15.8	13.7	18.2
	ERA5-Land	16.4	12.4	12.2
	CPRCMs ensemble	17.8 (± 4.0)	16.4 (± 3.5)	15.4 (± 3.7)
	RCMs ensemble	17.0 (± 4.3)	17.6 (± 3.7)	16.4 (± 3.2)
Persistence (days)	UERRA	8	9	7
	EOBS	9	7	11
	ERA5-Land	10	7	7
	CPRCMs ensemble	10 (± 2)	9 (± 2)	8 (± 1)
	RCMs ensemble	10 (± 2)	9 (± 2)	8 (± 1)

For the two simulated datasets, the inter-model spread (standard deviation of mean HW metrics produced by each ensemble member) is reported in brackets

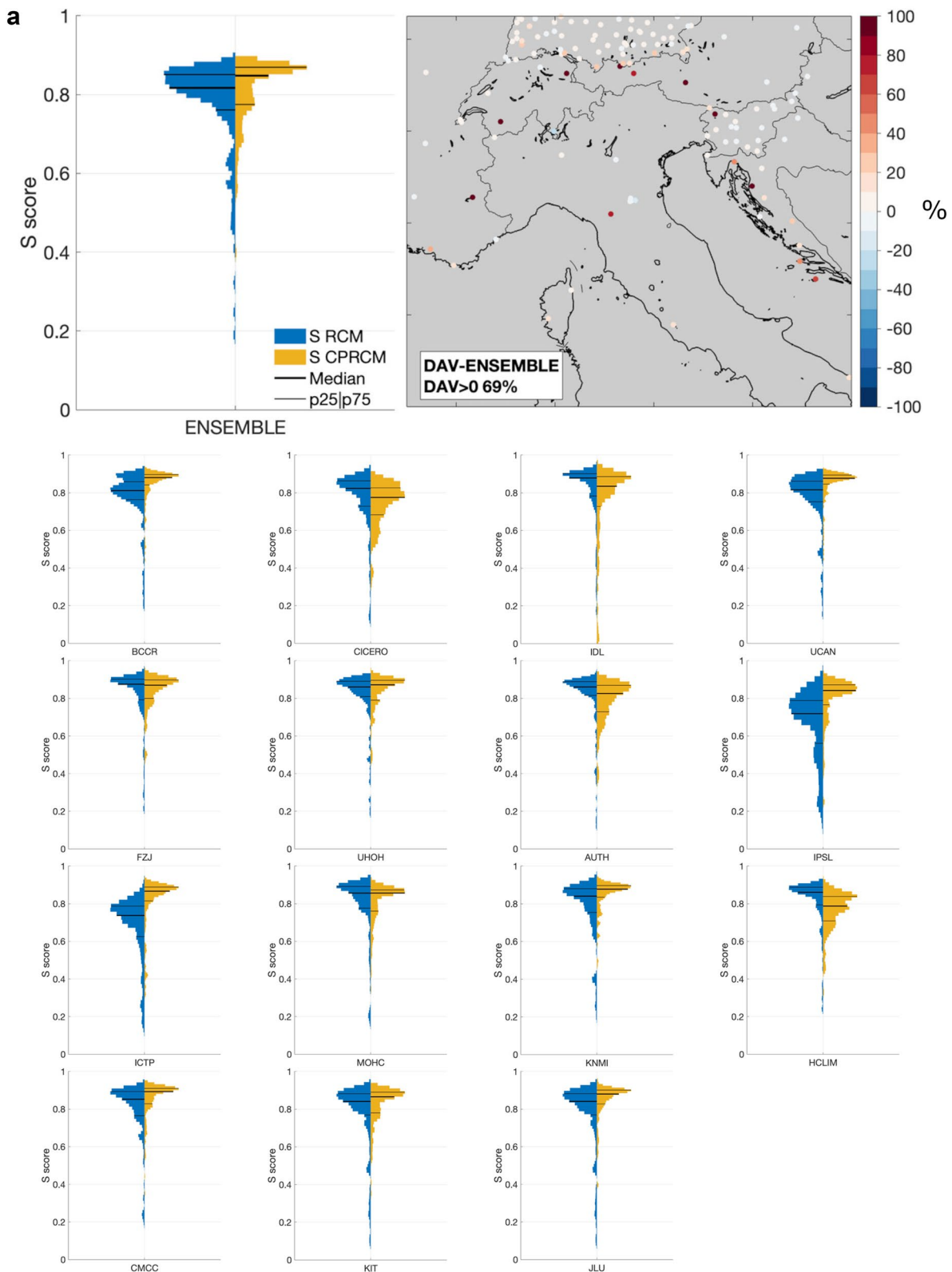


Fig. 5 Upper panels: RCMs and CPRCMs S score PDFs built considering all the reference sites (left). Percentage DAV in correspondence of the selected reference sites (right). Bottom panels: RCMs and CPRCMs S score PDFs built considering all the reference sites for all

the ensemble members. DAV computed on the entire distribution of evaluation period summer seasons daily Tmax is shown in panel (a) and only on the distribution right tail (90th–99th percentiles) in panel (b)

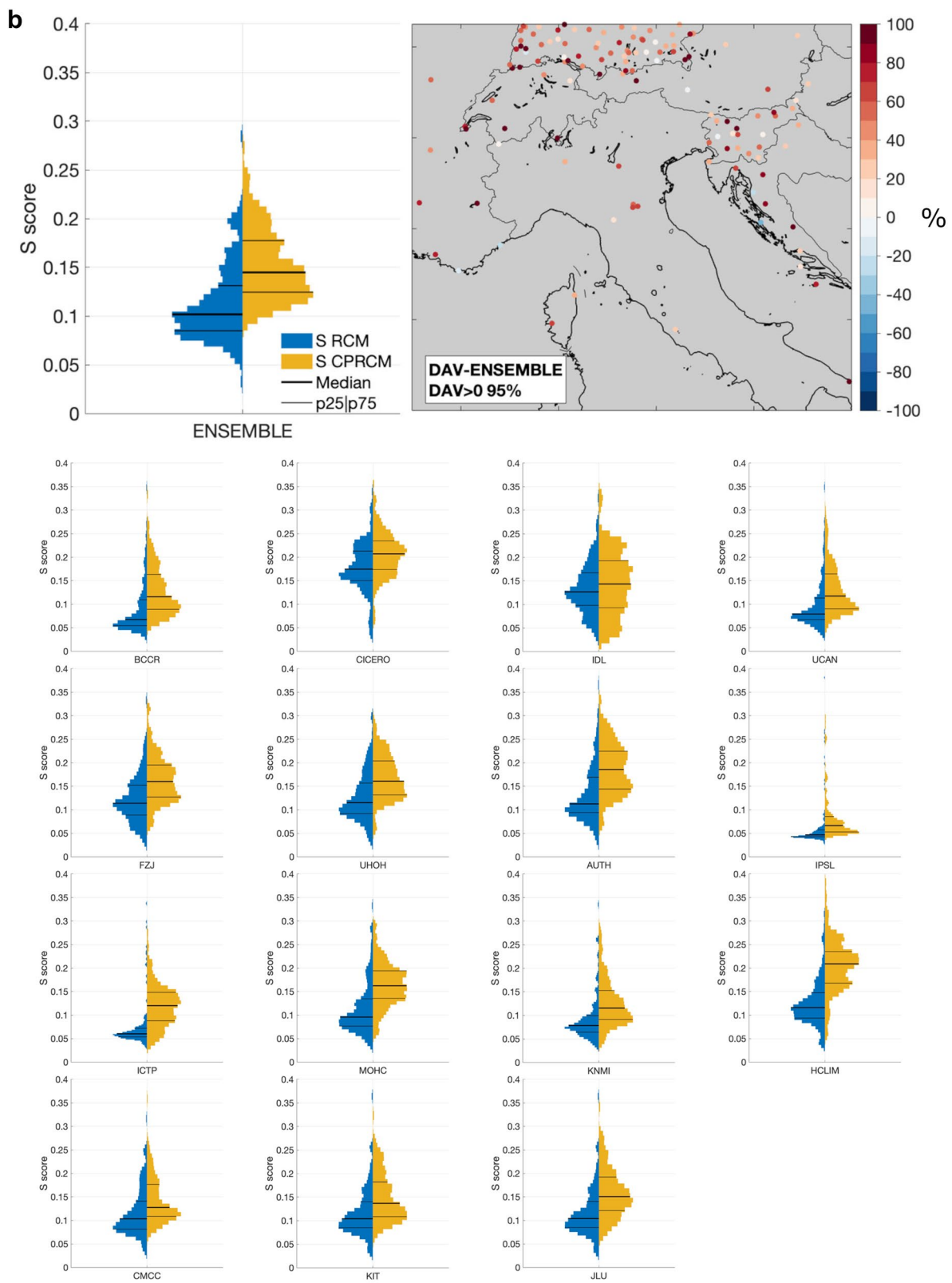


Fig. 5 (continued)

S scores characterizing the driving RCMs (median ~ 0.7) compared to the cases where a detrimental impact of the CP-scale results. In these latter cases, the driving RCMs already show satisfactory performance with a high S score median, sometimes close to 0.9, as for HCLIM, AUTH, and IDL models.

A larger CP-scale added value in terms of both the number of percentage reference sites with $DAV > 0$ (95%) and a generally higher DAV results when considering only the right tail summer seasons Tmax distribution (Fig. 5b). In this latter case, we can observe all the ensemble members producing higher S score at CP-scale than the nonCP-scale counterpart. This signals a generalized improved representation of temperature extremes over the reference sites considered.

It is now interesting to explore if, and to what extent, the added value in CPRCMs is due to a grid cell height closer to that of the reference station, as a result of the increased resolution. Since the systematic height difference shifts frequency histograms, affecting DAV, the same analysis is performed taking into account the nearest neighbor's height difference of both RCMs and CPRCMs with reference to station height. A first-order approximation is used according to a standard lapse rate of $0.0065\text{ }^{\circ}\text{C/m}$. As expected, a height correction reduces the CPRCMs added value in the sites located at higher elevations (Fig. SM 6). Height correction leads to a reduction of a few percentage points of the ensemble DAV computed over the entire Tmax distribution, moving from 69 to 66% of reference sites with positive DAV, with a similarly modest shift exhibited by the vast majority of models. Thus, there is an indication of genuine added value by the CPRCMs, not just related to the better representation of the station height. Though a height correction is commonly proposed in the evaluation of different resolution simulations, it should be mentioned that this does not systematically ensure a more sensible comparison. The lapse rate is consistently and non-linearly affected by local-scale features. Furthermore, the added value of higher resolution cannot be considered only belonging to improved representation of topography; it entails changes in simulating thermodynamic and dynamic features. These aspects make it challenging to disentangle the role of increased resolution vs. the role of improved physics, as they are inextricably linked. Finally, we test another DAV configuration, this time according to a grid node-by-grid node approach, following Careto et al. (2022) and shown in Figure SM 7a. Here, both ensembles are remapped and adiabatically adjusted to the EOBS grid and compared to grid-scale (instead of point-scale) observed values. According to this, CPRCMs ensemble produces a slightly detrimental effect mainly over the flat terrain of Po valley. In fact, considering distributions built on S scores from each subdomain grid node and from all the ensemble members, we can observe that only over the Alps

subdomain CPRCMs confirms an added value still producing higher S scores than RCMs (SM 7b).

3.2 Surface energy balance

In this section, we assess km-scale modulation on HWs heat fluxes partitioning. Figure 6 shows spatially averaged hourly time series of latent heat flux differences between RCMs and CPRCMs during HWs. Time steps where at least one of the two represents an HW are selected. In cases where RCM hourly time resolution is not available (i.e., CMCC and KIT RCMs) a 3-hourly mean is performed on the corresponding CPRCM hourly time series. In this analysis, HWs from 2000 are also included; these were not considered in the previous analyses as no HW was reproduced in the reference products. Figure 6 shows positive differences indicating larger latent heat in the RCMs excluding CMCC and KNMI (over Alps) and UHOH (over Po valley). These patterns are consistent with those resulting from previous temperature analyses.

In fact, RCMs showing large Tmax increases moving to the km-scale show also remarkable differences in latent heat flux. Namely, for IPSL, ICTP, MOHC, KNMI, and KIT simulations the difference between RCMs and CPRCMs can be as large as about 150 W/m^2 . This latter value in relative terms signals a consistent modification, considering that summer season latent heat flux peaks rarely exceed 350 W/m^2 .

Figure 7 summarizes the relationship between HWs Tmax and heat fluxes as represented by the Bowen ratio ($Br = \text{sensible heat} / \text{latent heat}$) for CPRCMs and RCMs ensemble means. Br gives a basic idea about the different partitioning of heat fluxes, which is mostly, but not only, driven by different soil moisture availability. In Fig. 7 we show Tmax vs. Br scatterplots for each subdomain, consisting of spatially and temporally averaged Tmax and Br time series of the three HWs for the two resolutions. Comparing CPRCM and RCM ensembles, drier-warmer conditions characterize CPRCM ensemble. In the presence of drier soils (i.e., Po valley) with higher Br, we observe a larger modulation in terms of both Br (from 4.5 to 7.5) and Tmax about $1.5\text{ }^{\circ}\text{C}$ warmer in the CPRCMs ensemble. In the Adriatic region a Br shift from 2.2 to 3.8 leads to higher Tmax in the CPRCMs ensemble of about $1\text{ }^{\circ}\text{C}$. Lastly, the Alps subdomain is the region showing the least modulation for both Br which moves from 0.8 to 1, and Tmax (less than $1\text{ }^{\circ}\text{C}$). This feature indicates stronger land–atmosphere coupling over dry soils, where sensible heat flux largely prevails over latent heat flux and to a larger extent in the CPRCMs ensemble.

Figure 8 shows results for the evaporative fraction (evapfr), another metric widely used to characterize the strength of land–atmosphere coupling (Knist et al. 2017; Careto et al. 2018). To characterize spatial and inter-model

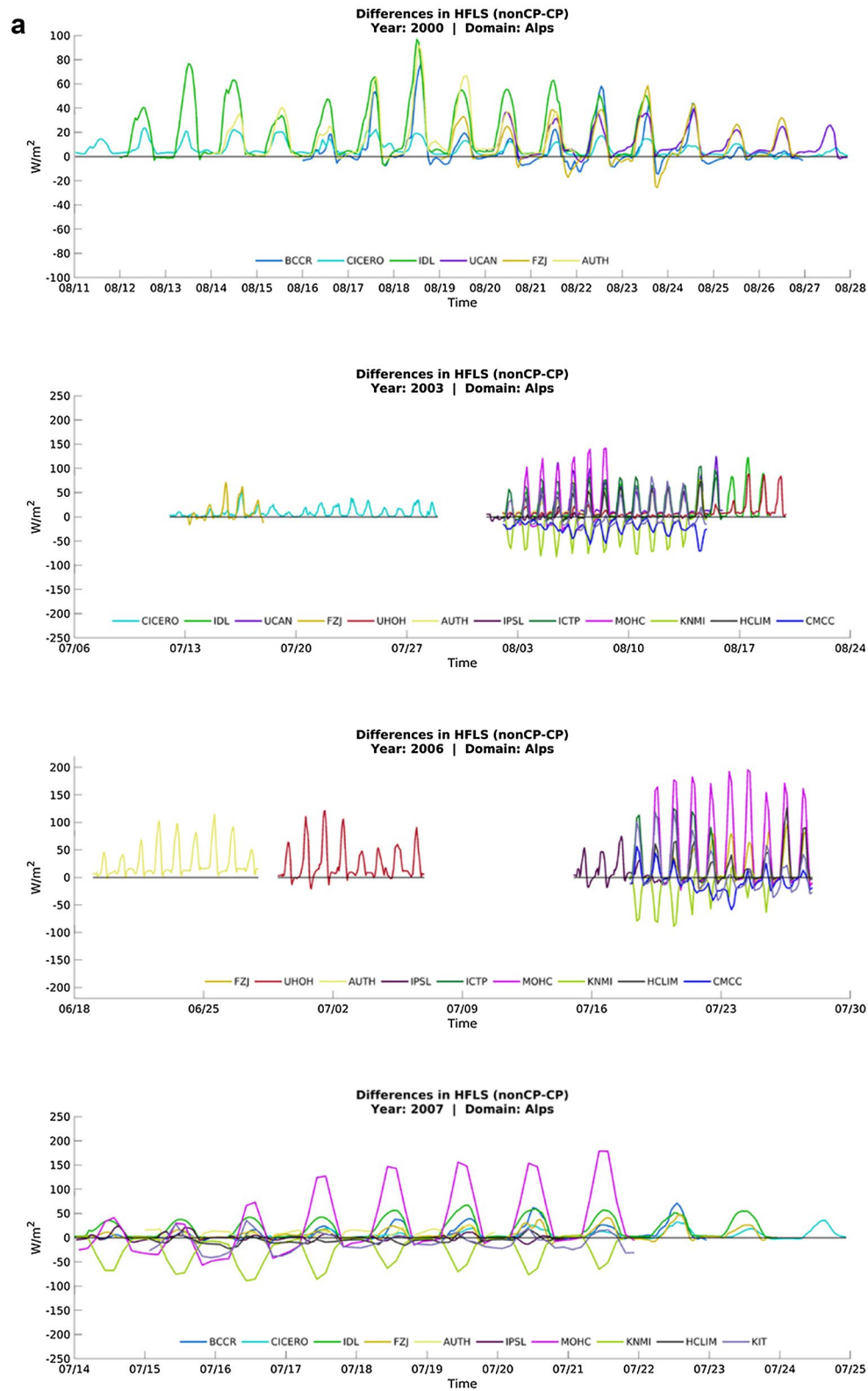


Fig. 6 Spatially averaged hourly (3-hourly if hourly not available) time series of differences in latent heat flux between RCMs (nonCP) and CPRCMs (CP) during HW events. Panels from left to right show the different domains whereas along the lines results for different

HW events are shown. For each model, only time steps where at least one of the two resolutions reproduced an HW event are considered. Only time steps with heat fluxes > 0 are shown. Results are shown for the three subdomains: Alps (a), Po valley (b), and Adriatic (c)

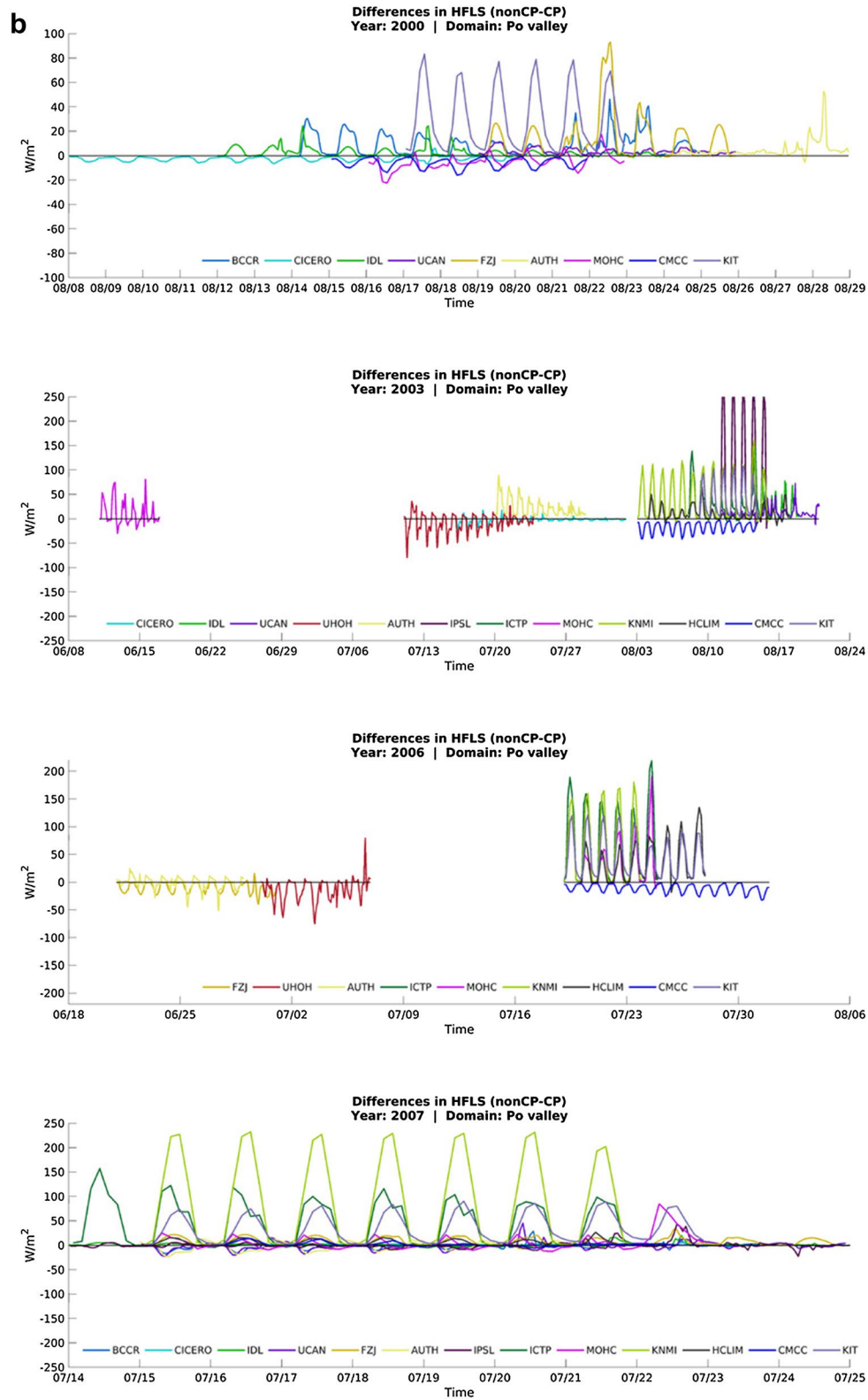


Fig. 6 (continued)

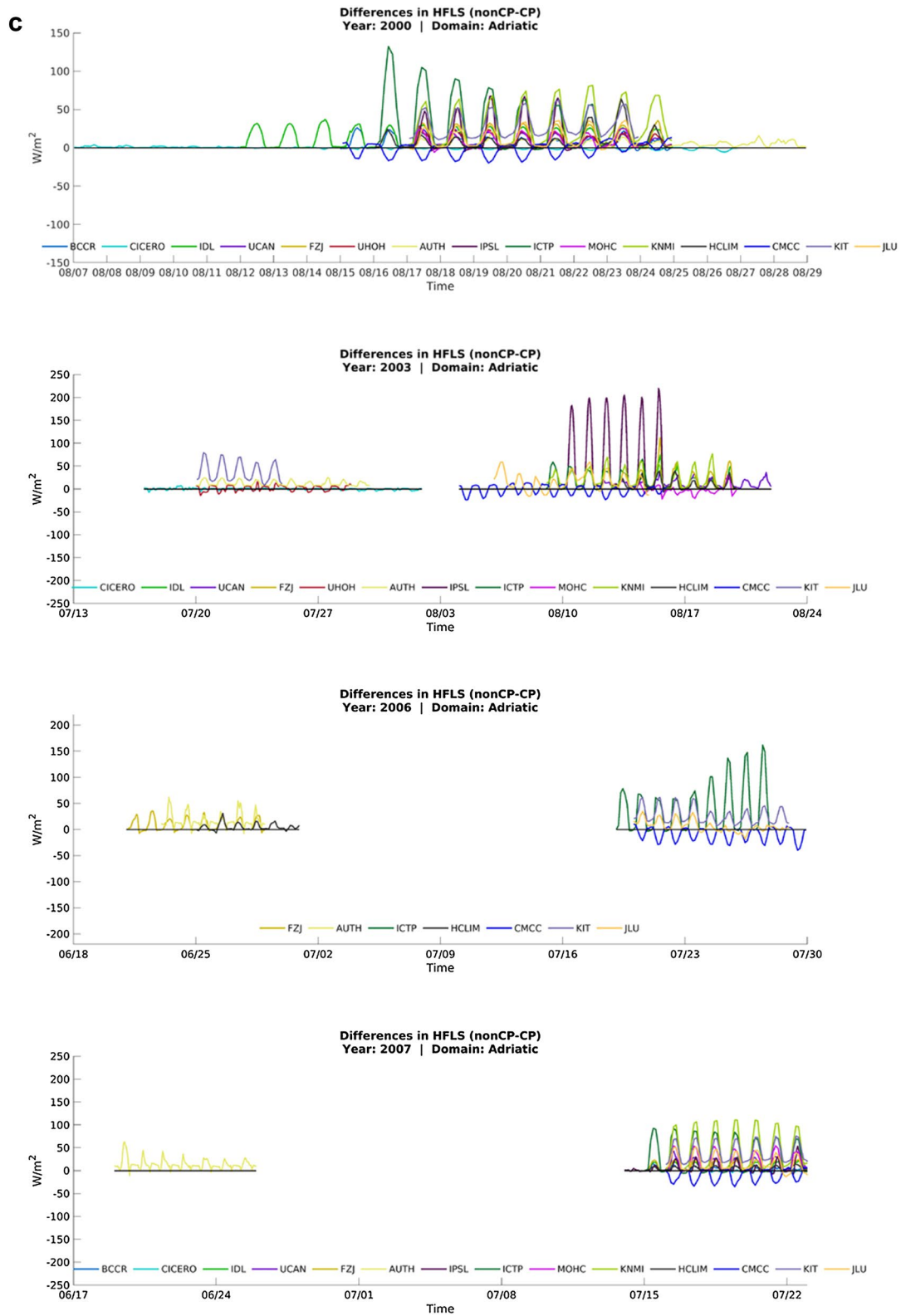


Fig. 6 (continued)

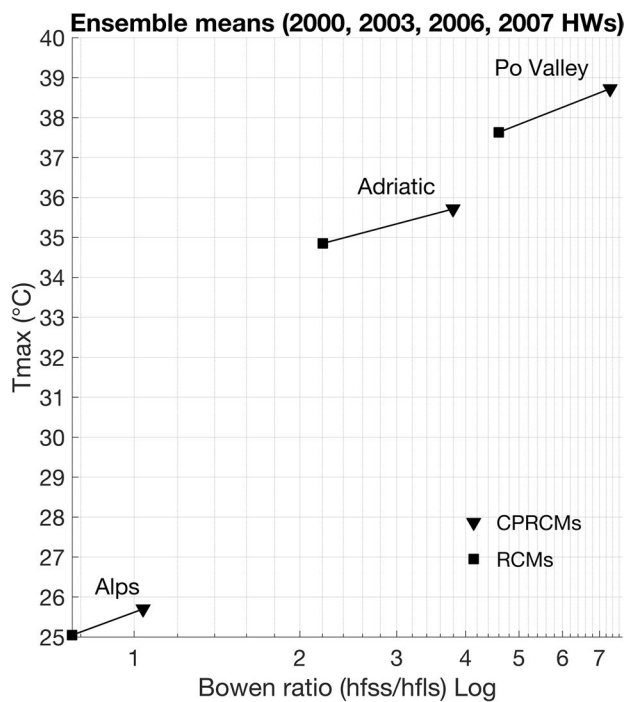


Fig. 7 HWs maximum temperature as a function of the Bowen ratio (ratio between sensible and latent heat fluxes) for the RCMs (squares) and CPRCMs (triangles) ensemble means and for the three subdomains. Values consist of spatial averages. The Bowen ratio is defined only considering time steps with heat fluxes > 0

variability results refer to an extended area (same as Fig. 4) which includes the three subdomains and all the models. Differently from the previous analyses involving heat fluxes CICERO simulations (see Fig. SM 8 caption). Results in Fig. 8 refer to the most intense HW event of the 2003 summer season (2–14 August). Over plain, the two resolutions show large differences with evapfr for CPRCMs ranging between 0.1 and 0.2 whilst RCMs ensemble ranges about 0.2 and 0.4. Within a generalized strong lower evapfr the most striking differences are found for the IPSL, ICTP, and MOHC simulations confirming that the km-scale modulation does not present a model dependency involving different models and downscaling approaches. Noteworthy is also the larger inter-model variability within the RCMs ensemble compared to the CPRCMs ensemble characterized by a convergence toward low evapfr. This is also considering simulations belonging to the same modeling consortium (e.g., WRF IPSL and BCCR RCMs sticking out compared to the other WRF RCMs). Lower CP-scale evaptr tendency is partially overturned for the KNMI simulations where CPRCM shows higher evapfr than in the RCM. However, this effect is restricted to complex orography areas. Moreover, for KNMI CPRCM and RCM are two different models causing higher independence compared to models sharing the same numerical configuration in the two resolutions. Finally, CP-scale

signature is confirmed extending even outside HW conditions as it can be observed in Fig. SM 8 where the mean evapfr is computed considering all the evaluation period summer seasons.

3.3 Soil moisture

In this section, we explore differences in soil moisture content between CPRCMs and RCMs. Figure 9a, b show representative 2003 HW mean volumetric soil moisture for the CPRCMs and RCMs, respectively. All the simulated soil moisture values belong to the top-soil layer, excluding ICTP RegCM. For this latter, which provides several soil layers, is selected the depth closest to the 0.10 m (0.12 m) characterizing the majority of models. Simulated soil moisture datasets have been interpolated on a common grid of 3 km resolution for CPRCMs and 15 km resolution for the RCMs. The reference products ESSMRA and ERA5-Land reanalysis (top-left and top-central panels respectively) are shown on their native grid resolution (3 km and 9 km respectively). These two products show substantially different soil moisture values during the 2003 event, and even more when considering the summer (JJA) climatology for the reference period (Fig. SM 9). It is a challenge to disentangle to what extent differences are driven by different soil layer depths (0–3 cm and 0–7 cm for ESSMRA and ERA5-Land respectively) or by structural land surface modeling system differences. For sake of comparability between simulated and reference values, soil moisture in models, originally provided in $\text{kg} \cdot \text{m}^{-2}$, is converted to volumetric soil moisture ($\text{m}^3 \cdot \text{m}^{-3}$) according to Bauer-Marschallinger and Stachl (2019):

$$\text{SM}[\text{m}^3/\text{m}^3] = \text{SM}[\text{kg}/\text{m}^2] * 0.001 * 1/d$$

where d is the thickness of the soil layer in meters. The factor 0.001 is due to the assumption that 1 kg of water represents 1000 cm^3 , which is 0.001 m^3 . However, even with the same units, a direct comparison between the model's soil moisture and reference products is hindered by different top-soil layer depths between models and reanalysis. Also, top-soil layer depth varies among models as a result of different land surface models employed by the different modeling consortia. Taking into account these limitations, it is possible to compare soil moisture among a large part of the models. These do not include KNMI, for which soil moisture data is not available. Moreover, KIT runs have a different top-soil layer depth between the CPRCM and RCM, and JLU which performs a one-step downscaling. Excluding the CMCC, all the CPRCMs tend to get drier than the RCMs (cf. Fig. 9a, b). CICERO and to a lesser extent UHOH and AUTH WRF runs present evident dry conditions already on the RCM, especially over the flat terrain of Po valley. In these cases, CPRCMs tend to preserve almost totally dry conditions,

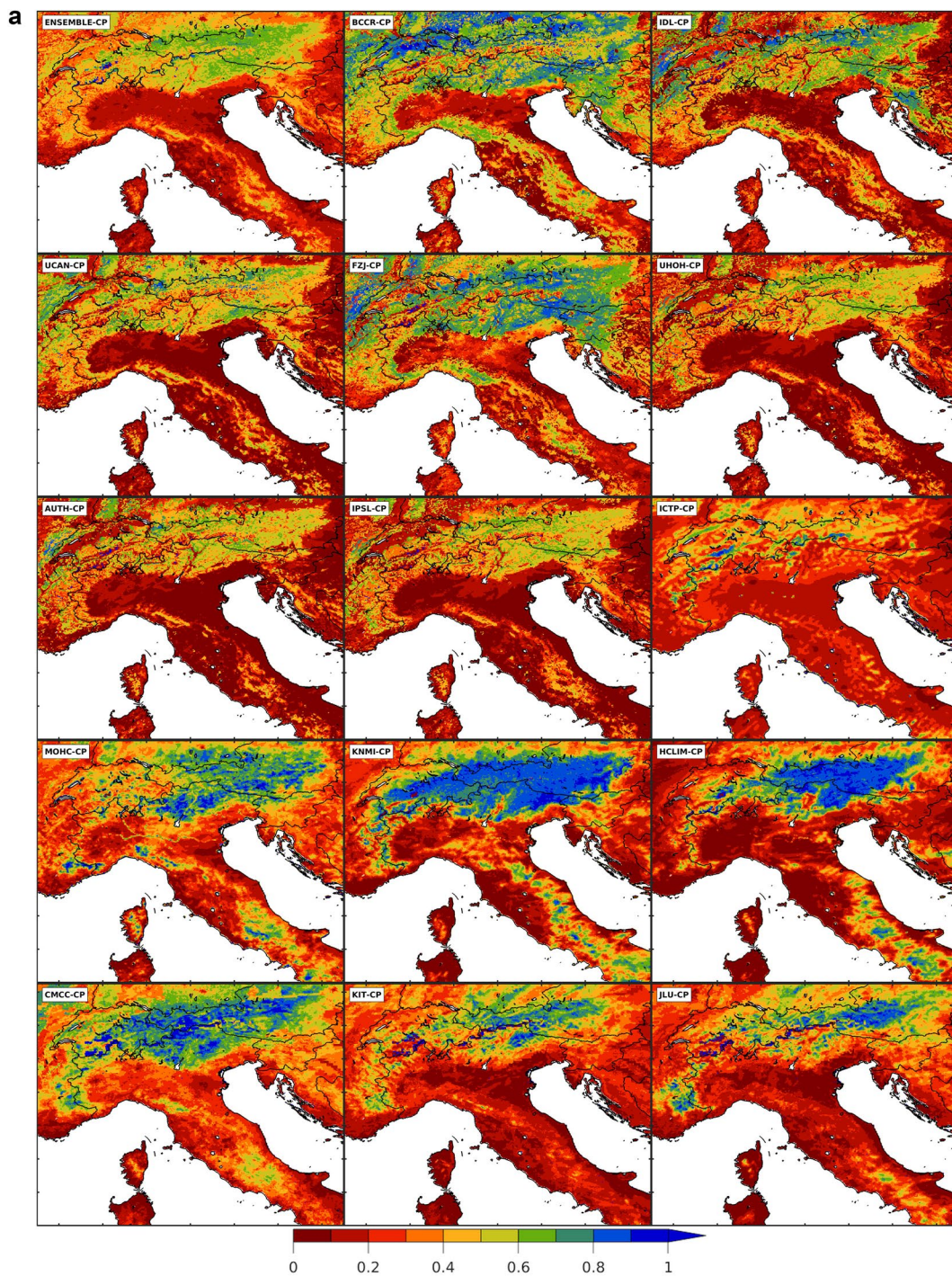


Fig. 8 Spatial patterns of mean evaporative fraction for the 2003 HW over a representative domain including the Alps, Po valley, and Adriatic region. CPRCMs and RCMs are shown in panels (a, b) respectively

with a subsequent irrelevant alteration of HW maximum temperature (Fig. 2). Supplementary materials Fig. SM 9a and SM 9b show the same analysis, but averaging JJA daily soil moisture data over the entire evaluation period summer seasons. Here, similar km-scale modulation patterns can be observed for the majority of models, confirming

that CPRCMs modulation is not limited to HW events. In Fig. 10, we show the temporal evolution during the evaluation period of percentage differences between CPRCMs and RCMs soil moisture. Again, we only consider comparable models in terms of soil layer depth. With respect to Fig. 9a, b, Fig. 10 excluded CMCC runs providing a very shallow

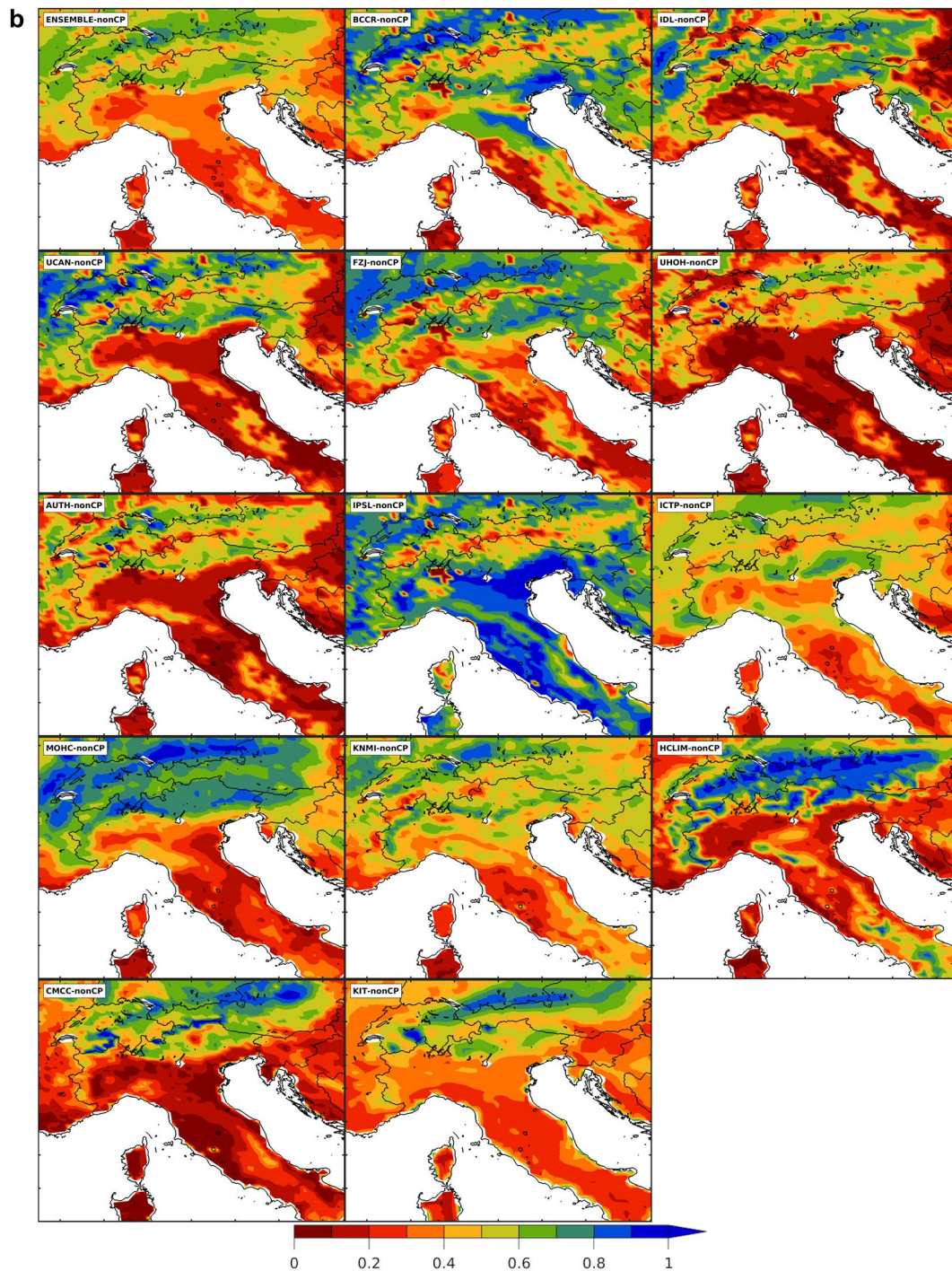


Fig. 8 (continued)

top-soil layer with a day-to-day variability not comparable to the other models; KIT runs which have two different soil layer depths between CPRCM and RCM, and MOHC runs are excluded because of too large differences between CP and non-CP runs despite employing the same land surface model parameterization but different configurations. These large differences in MOHC come from the non-CP run being

closer to the UK Met Office global climate configuration and the CP run being closer to the weather-like configuration of the same model. The CP run has too much runoff due to this configuration difference plus too little canopy interception, which makes it very dry in the summer months (Halladay et al. 2021).

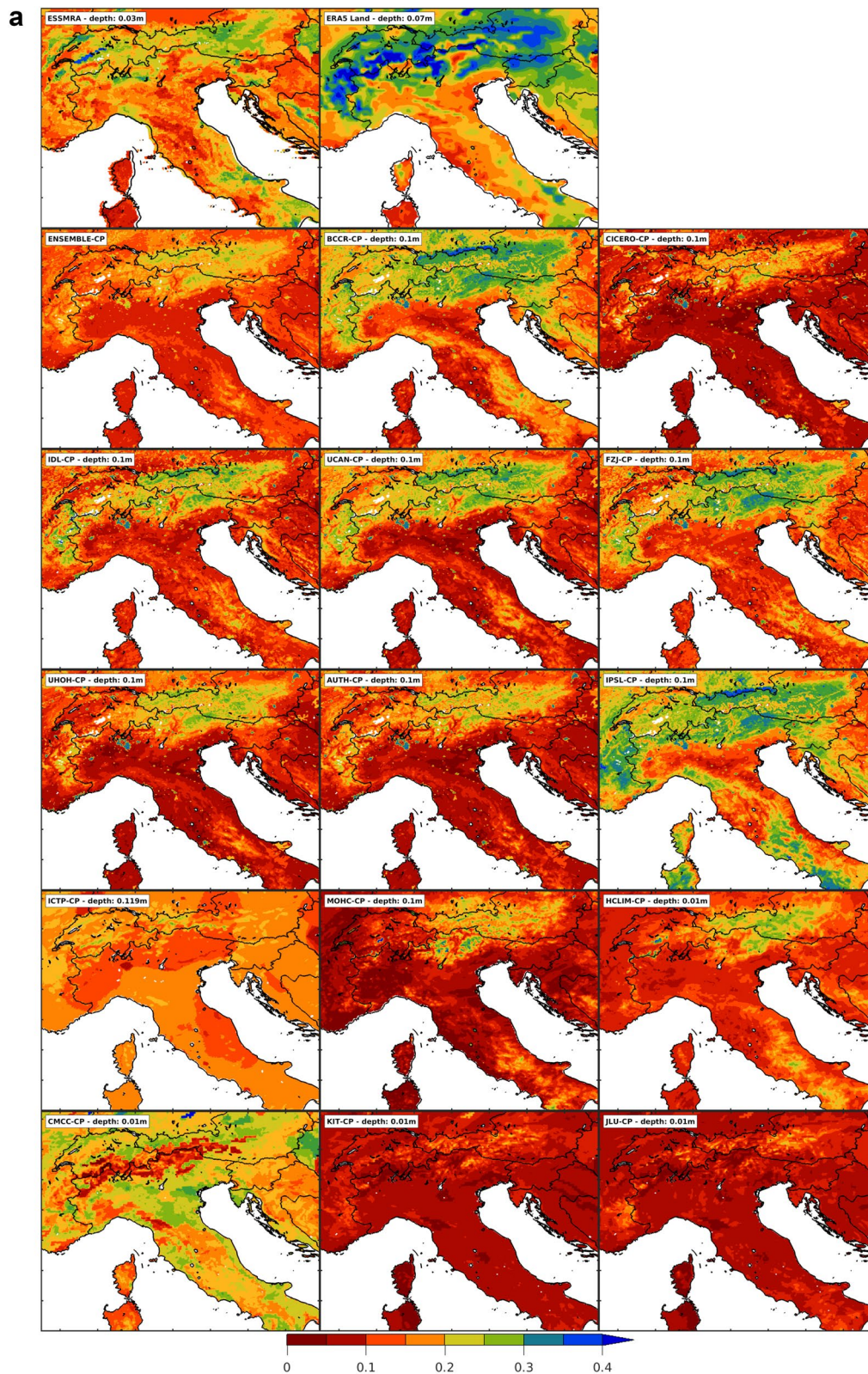


Fig. 9 As in Fig. 8 but for the mean volumetric soil moisture. In the upper part of each panel is reported the depth of the soil layer providing the soil moisture for the different models and reference products (ESSMRA and ERA5-Land reanalysis). Units are m^3/m^3

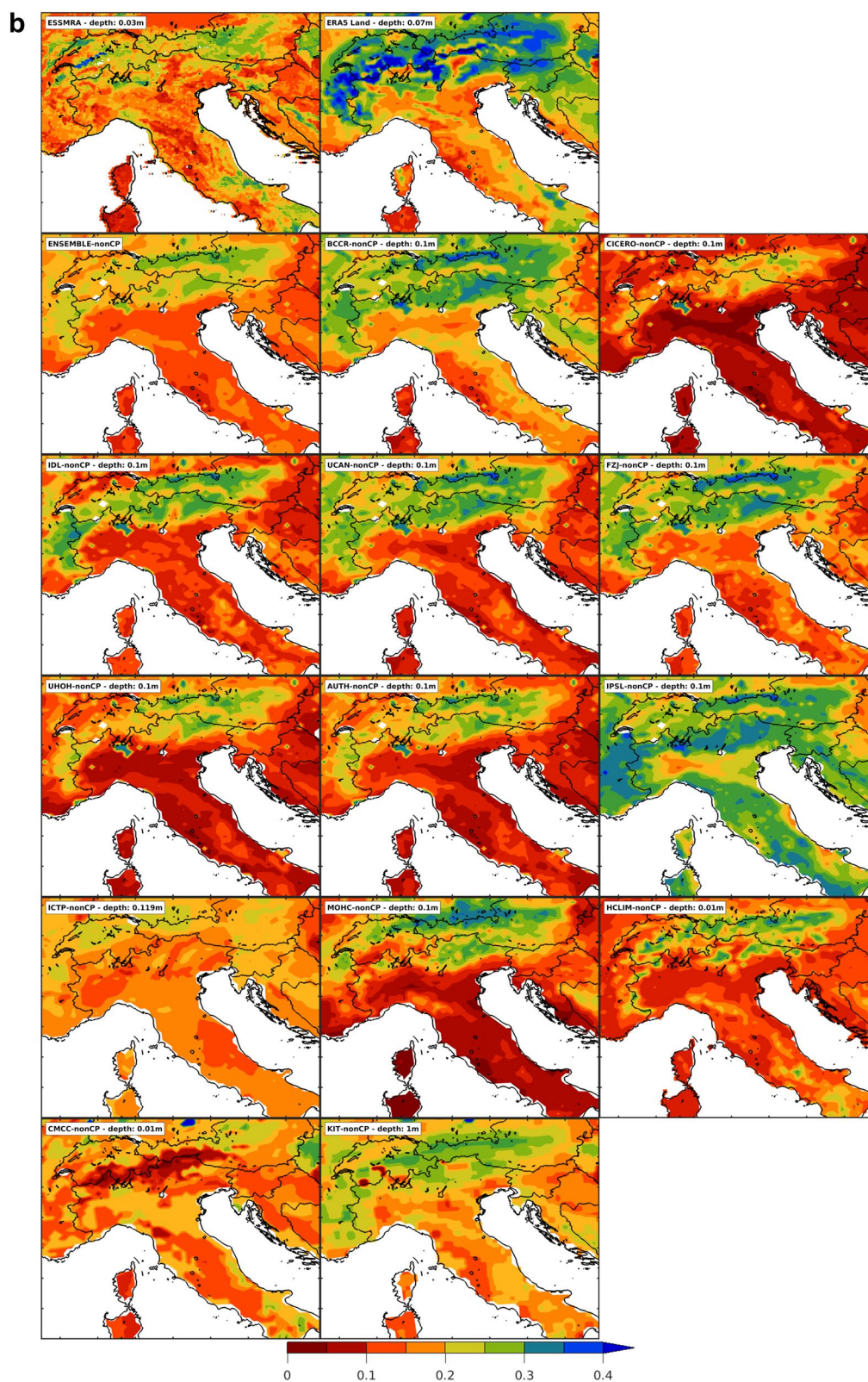


Fig. 9 (continued)

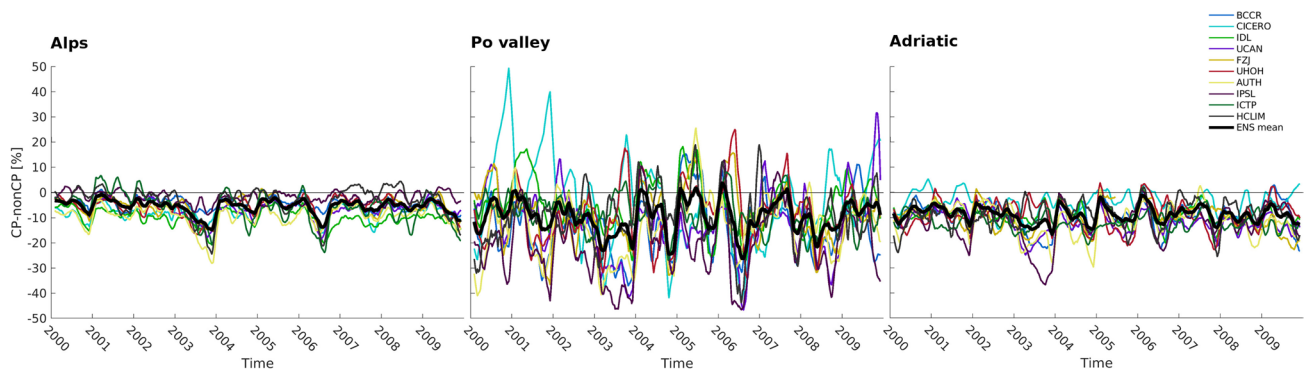


Fig. 10 Spatially averaged time series of the percentage difference between CP and non-CP simulations volumetric soil moisture content for the three domains. Time series consist of running means with a

temporal window of 15 days and consider the entire evaluation experiment period (2000–2009) summer seasons

Over the Alps domain, CPRCMs show lower soil moisture than corresponding RCMs with an ensemble mean difference ranging from -5 to -15% . Two main peaks reporting larger differences can be observed during the 2003 and 2006 summer seasons, characterized by the two most intense HW events. Larger differences combined with noisier patterns can be observed over Po valley.

Here, low soil moisture values contribute to determining the large variability of percentage differences, by combining very small numbers into fractions. Negative differences between RCMs and CPRCMs prevail, with some positive values resulting from the driest CICERO runs. In what concerns the 2003 and 2006 summer seasons, the ensemble mean shows a negative difference reaching about -25% with some models down to -40% . The Adriatic region domain shows intermediate characteristics between the Alps and Po valley domains.

Results obtained so far suggest an enhancement of the HWs by the CPRCMs compared to the RCMs. However, it is difficult to state if these signals constitute an improvement. This is because HW events are rare and inferences are constrained by the small sample size. For better framing of soil moisture modulation occurring during HWs, we depict in Fig. 11a the annual cycle of soil moisture in the CPRCMs vs. the RCMs. In the case of a more realistic soil moisture annual cycle, it can be argued that the HW representation is also improved. Figure 11a shows CPRCMs and RCMs volumetric soil moisture monthly means over the three domains. Simulations are compared to the topsoil layer (7 cm depth) of ERA5-Land, and ESSMRA (3 cm depth) are considered as reference products. The majority of models have a 10 cm depth topsoil layer (see Fig. 9), and in those cases ERA5-Land better matches than the ESSMRA (3 cm depth). For COSMO (CMCC, KIT (CP), and JLU) and HCLIM simulations, ESSMRA represents the best matching reference product.

Over the Alpine domain, ERA5-Land shows an annual cycle characterized by a dry peak in late winter and a wet peak in late spring. A similar annual cycle with smaller values is shown by ESSMRA reanalysis. Compared to ERA5-Land, all models (except HCLIM) miss the spring peak, leading to a too-dry summer (relative to their corresponding winter level) likely driven by a misrepresentation of snow melting. Simulated annual cycles show dry conditions peaking during summer months and wettest conditions in winter months. HCLIM model, having a shallower topsoil layer depth (1.0 cm) reproduces the reference annual cycle, but it exaggerates annual variability. Considering the ensemble means, small differences between CPRCMs and RCMs characterize winter and spring months. Differences get larger during summer. In this regard, it can be observed how the drier CPRCMs ensemble means would be mostly determined by the particularly dry KIT and JLU simulations. It is worth recalling that KIT CPRCM and RCM soil moisture are not comparable (1 cm vs. 1 m soil layer depth, respectively). Besides these two models, the MOHC model is the one showing the largest difference between the two resolutions, with a drier summer season and an early dry peak (from August to July) at the CP scale. The WRF ensemble shows a small spread across members and a reduced summer season drying when moving to the km-scale. In this regard, there is a clear model-specific behavior, especially for the Alps, where different layer thicknesses can be seen as at least partially contributing to this model-based differentiation.

Po valley and Adriatic domains show similar soil moisture annual cycles characterized by an evident summer dry peak. ERA5-Land and ESSMRA show the driest conditions in July, whereas CPRCMs and especially RCMs show dry conditions peaking in August. Both the CPRCMs and RCMs show dry biases during the entire annual cycle, exacerbated from late spring through summer by the CPRCMs. Especially over Po valley, CPRCMs

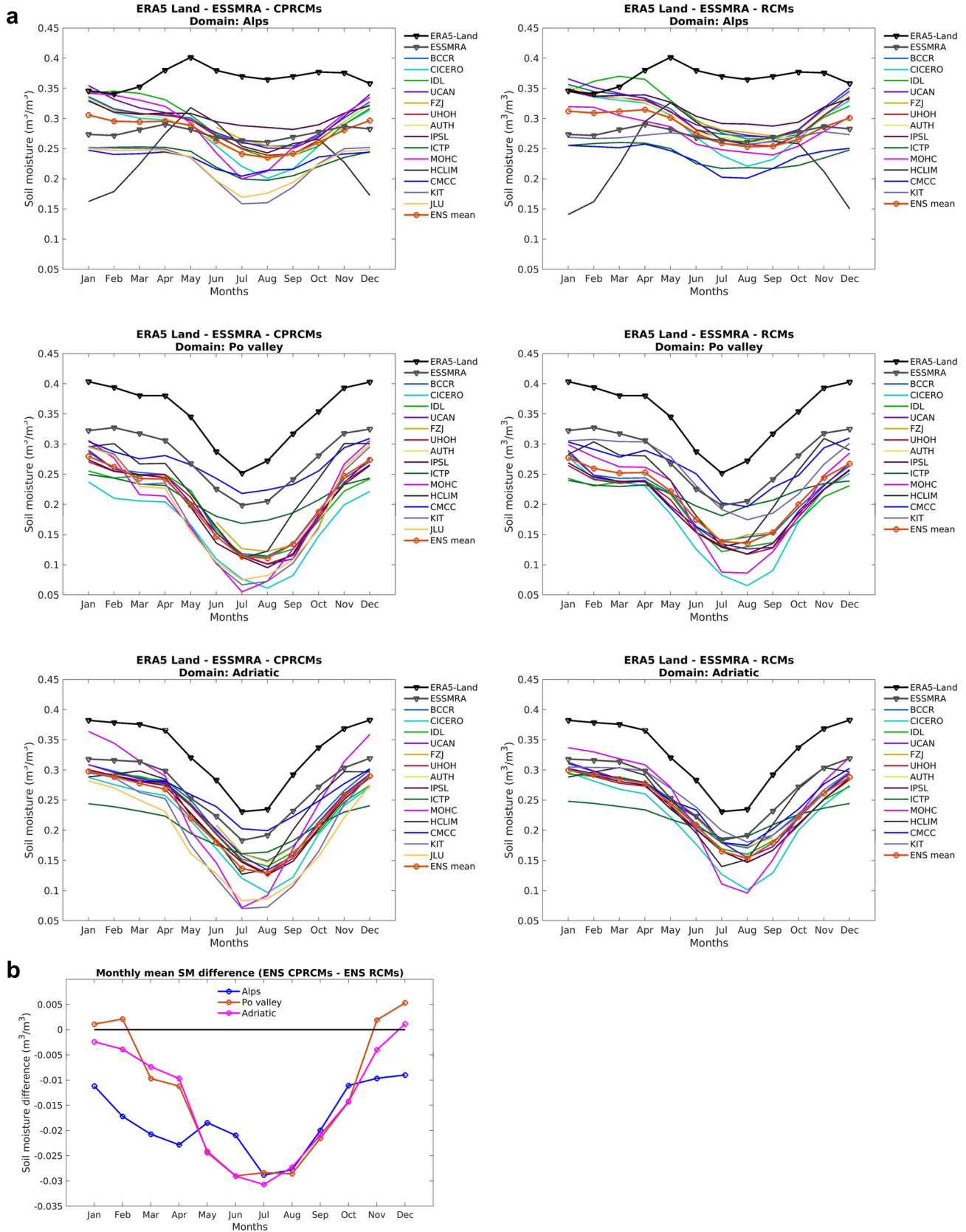


Fig. 11 Monthly means of volumetric soil moisture content over the three domains. Reference products ERA5-Land (0.07 m soil layer depth) and ESSMRA (0.03 m soil layer depth) overlaid to CPRCMs (left) and RCMs (right) and related ensemble means (**a**). Differences of volumetric soil moisture content monthly means between CPRCM and RCM ensembles (**b**). Note that for FZJ WRF, soil moisture is available only for the summer season

are also characterized by a steeper increase in monthly values during autumn and early winter. Confirming previous results, the CMCC model is generally very close to the ESSMRA reference product (especially over flat territories) and shows a different modulation between the two resolutions, with a more emphasized summer drying in the RCM compared to the CPRCM. In July and August, CMCC CPRCM shows higher soil moisture than the corresponding RCM, resulting closer to ERA5-Land but too wet considering the ESSMRA dataset.

Table 3 summarizes the monthly mean soil moisture Pearson correlation coefficient between CPRCMs and RCMs and the two reference products (ERA5-Land and ESSMRA). Over the Alpine subdomain, we can observe substantial differences according to the different reference products considered. When ERA5-Land is considered as a reference, both RCMs and CPRCMs show a negative correlation, shifting to a positive and generally significant correlation when ESSMRA dataset is considered as a reference. HCLIM shows an opposite behavior with a significant positive correlation with ERA5-Land. In any case, it must be underlined the large difference between the two reference datasets. Here, besides the different layer depths also differences in precipitation regime and recycling in the two reanalysis systems could play a role as well. Over the other two subdomains, both CPRCMs and RCMs show a positive significant correlation with both reference products.

Finally, in Fig. 11b we test if the CPRCMs drier signal is limited to the summer season or affects the entire year deriving differences in monthly mean soil moisture between CPRCM and RCM ensembles. Here, we can observe, especially over Po valley and Adriatic subdomains, a distinct annual cycle of soil moisture differences, with lower values close to zero in November, December, January, and February and a sharp increase of differences during summer months. This points out that the CP-scale signal albeit not limited to the summer season is most prominent during the warm semester.

In conclusion, CPRCMs are still drier than their non-CP counterparts beyond canonical summer months affecting the entire warm semester and their spread is large. This source of uncertainty requires deeper investigations also considering relevant knock-on implications for precipitation via the soil-moisture precipitation feedback whose characterization goes beyond the scope of the present study. Nonetheless, a large source of uncertainty comes also from reference

products considered, presenting a large spread and being characterized by considerable structural differences.

3.4 Dry spell length

Figure 12a, b present a comparison between CPRCMs and RCMs summer months mean dry spell length (DSL) considering the entire evaluation period summer seasons. As a reference, two different observational-based precipitation datasets are considered: EURO4M (Isotta et al. 2014) from $\sim 43^\circ\text{N}$ northward and GRIPHO (Fantini 2019) from $\sim 43^\circ\text{N}$ southward.

DSL is derived considering daily accumulated precipitation, where a dry day is characterized by precipitation lower than 1 mm.

Consistent with what is observed for soil moisture, substantial differences can be observed. CPRCMs ensemble mean introduces, on the one hand, an improved representation of the topography-driven spatial patterns, on the other hand, it also introduces a remarkable extension of DSL compared to the RCMs ensemble mean. Compared to reference products, this consists of a substantial overestimation of the observed DSL with RCMs ensemble showing mean DSL closer to the observations. Large differences between CPRCMs and RCMs DSL are particularly evident over flat terrain and coastline, where CPRCMs DSL doubles RCMs DSL. Even with large differences, all the models, excluding CMCC, present the km-scale version characterized by longer DSL. Focusing on the two models showing the largest temperature modulation between the two resolutions (ICTP and MOHC), ICTP shows also the largest difference between CPRCM and RCM DSL. Differently, the MOHC model does not present particularly high DSL alteration between the two resolutions. This fact suggests potentially different mechanisms underlying temperature alteration resulting in the two models. Moreover, unlike other models, ICTP km-scale runs show an improvement compared to the RCM where a consistent wet bias is overcorrected to a dry bias but of smaller magnitude. Figure 13 shows DSL alteration between the two resolutions and related deviation from the observations for the three domains and over the entire statistical distribution (empirical cumulative distribution function, ECDF). Here, to preserve as unaltered as possible the original daily precipitation statistics, no interpolation is performed. ECDFs are defined considering grid node-by-grid node DSL time series along the entire evaluation period summer seasons. Distinct modulation tendencies can be observed in the different domains. Again, the largest modulation signal appears over the flat terrain of the Po valley, where almost all members of the km-scale ensemble are shifted on the right side of the observed ECDF, indicating longer DSL over the entire statistical distribution. In contrast, observed ECDF is evenly distributed within the variability of RCMs ensemble. A

Table 3 Monthly mean soil moisture (upper soil level) Pearson correlation coefficients between CPRCMs and RCMs and two reference products (ERA5-Land and ESSMRA)

	r CPRCM ERA5-Land	r RCM ERA5-Land	r CPRCM ESSMRA	r RCM ESSMRA
Alps				
BCCR	−0.4	−0.46	0.61*	0.60*
CICERO	−0.31	−0.34	0.7*	0.68*
IDL	−0.4	−0.32	0.6 *	0.58*
UCAN	−0.5	−0.52	0.5	0.54
UHOH	−0.36	−0.41	0.63*	0.62*
AUTH	−0.42	−0.5	0.64*	0.60*
IPSL	−0.34	−0.34	0.57 *	0.64*
ICTP	−0.23	−0.32	0.78 *	0.63*
MOHC	−0.38	−0.48	0.72*	0.54
HCLIM	0.9*	0.86*	−0.00	−0.04
CMCC	−0.23	−0.17	0.81*	0.81*
KIT	0.21	0.36	0.82*	0.82*
JLU	−0.22	–	0.82*	–
ENSEMBLE mean	−0.26	−0.25	0.74*	0.69*
Po valley				
BCCR	0.95*	0.94*	0.96*	0.94*
CICERO	0.95*	0.95*	0.96*	0.96*
IDL	0.92*	0.92*	0.93*	0.93*
UCAN	0.93*	0.93*	0.95*	0.93*
UHOH	0.94*	0.93*	0.95*	0.94*
AUTH	0.95*	0.95*	0.97*	0.96*
IPSL	0.94*	0.88*	0.94*	0.86*
ICTP	0.97*	0.99*	0.98*	0.97*
MOHC	0.97*	0.94*	0.96*	0.95*
HCLIM	0.99*	0.98*	0.99*	0.98*
CMCC	0.95*	0.93*	0.95*	0.93*
KIT	0.96*	0.86*	0.97*	0.88*
JLU	0.95*	–	0.96*	–
ENSEMBLE mean	0.97*	0.95*	0.97*	0.96*
Adriatic				
BCCR	0.96*	0.95*	0.96*	0.95*
CICERO	0.95*	0.95*	0.95*	0.95*
IDL	0.93*	0.93*	0.93*	0.93*
UCAN	0.94*	0.92*	0.95*	0.93*
UHOH	0.94*	0.94*	0.95*	0.94*
AUTH	0.95*	0.94*	0.95*	0.94*
IPSL	0.97*	0.92*	0.96*	0.93*
ICTP	0.98*	0.99*	0.99*	0.99*
MOHC	0.98*	0.96*	0.99*	0.96*
HCLIM	0.99*	0.99*	0.99*	0.98*
CMCC	0.97*	0.96*	0.97*	0.96*
KIT	0.97*	0.90*	0.98*	0.90*
JLU	0.95*	–	0.97*	–
ENSEMBLE mean	0.97*	0.96*	0.98*	0.96*

Asterisks denote significant correlations (confidence interval at 95%)

similar modulation pattern, though with a lower magnitude, is evident over the Alps and Adriatic regions. In the upper part of the panels, we report DSL simulated and observed values for representative statistical moments. As already mentioned, the CPRCM ensemble shows statistics roughly doubling the observed values. The RCM ensemble presents more comparable values to the reference products in all the subdomains.

3.5 Forcing during HW and non-HW conditions

In this last section, we analyze the temporal evolution of relevant forcing variables during HW and non-HW conditions for two representative summers seasons and spatially averaged over the Po valley subdomain. Figure 14 shows an ensemble mean time series with horizontal lines representing the corresponding climatological mean derived over the evaluation period summer seasons. All the time series are daily means except for the PBL height (panel d) which has a three-hourly mean temporal aggregation.

The analysis involves the 2003 and 2007 summer seasons and the corresponding most intense HW events. The two seasons show interesting differences in terms of soil moisture-precipitation feedback nuances, characterizing the two resolutions. In 2003 we observe that drier CP-scale conditions are already set there at the beginning of the summer, with a persisting drier CP-scale regime throughout the summer season. Differences in precipitation in the two resolutions drive strong modulation of soil moisture in terms of both physical values and corresponding anomalies. We can observe a long-standing soil moisture-positive anomaly in June in the RCMs ensemble differently from the CPRCMs ensemble. The corresponding differences in heat fluxes partitioning affect T_{max} , with CPRCMs ensemble up to 3 °C warmer than the RCMs ensemble in mid-June and corresponding to a larger difference in daily precipitation. This is also combined with larger differences, in the PBL height between the two resolutions with substantially higher PBL limit in the CPRCMs ensemble up to several hundreds of meters.

It is noteworthy that differences in T_{max} progressively decrease (down to about 1–2 °C) starting from the beginning of August. This occurs regardless of the onset of an HW during which we observe slightly reduced differences between the two resolutions as they both get drier. These results suggest a relevant contribution of different soil moisture-precipitation feedbacks behind the CP-scale temperature modulation. Furthermore, it is noteworthy that the HW onset does not exacerbate temperature modulation. The case of the 2007 summer season represents perhaps an even more interesting case in terms of soil moisture-precipitation feedback in the two resolutions. Differently from the 2003

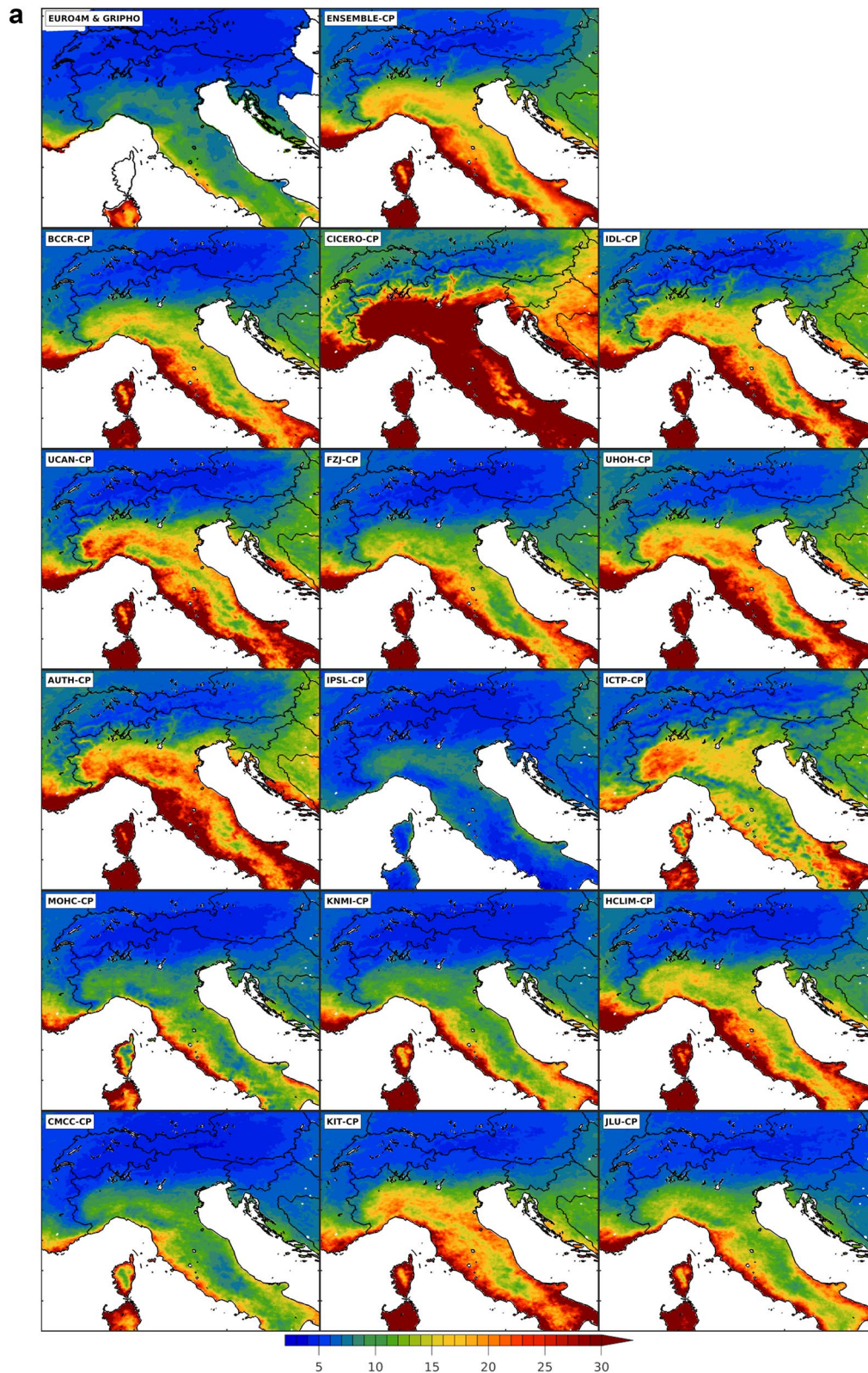


Fig. 12 Spatial pattern of mean dry spell length (DSL) over a representative domain including the Alps, Po valley, and Adriatic region for the CPRCMs (a) and RCMs (b). DSL considers the sum-

mer season's daily precipitation from 2000 to 2009. In the top-left panel results from the reference product (a merge of EURO4M and GRIPHO datasets) are shown. Units are days

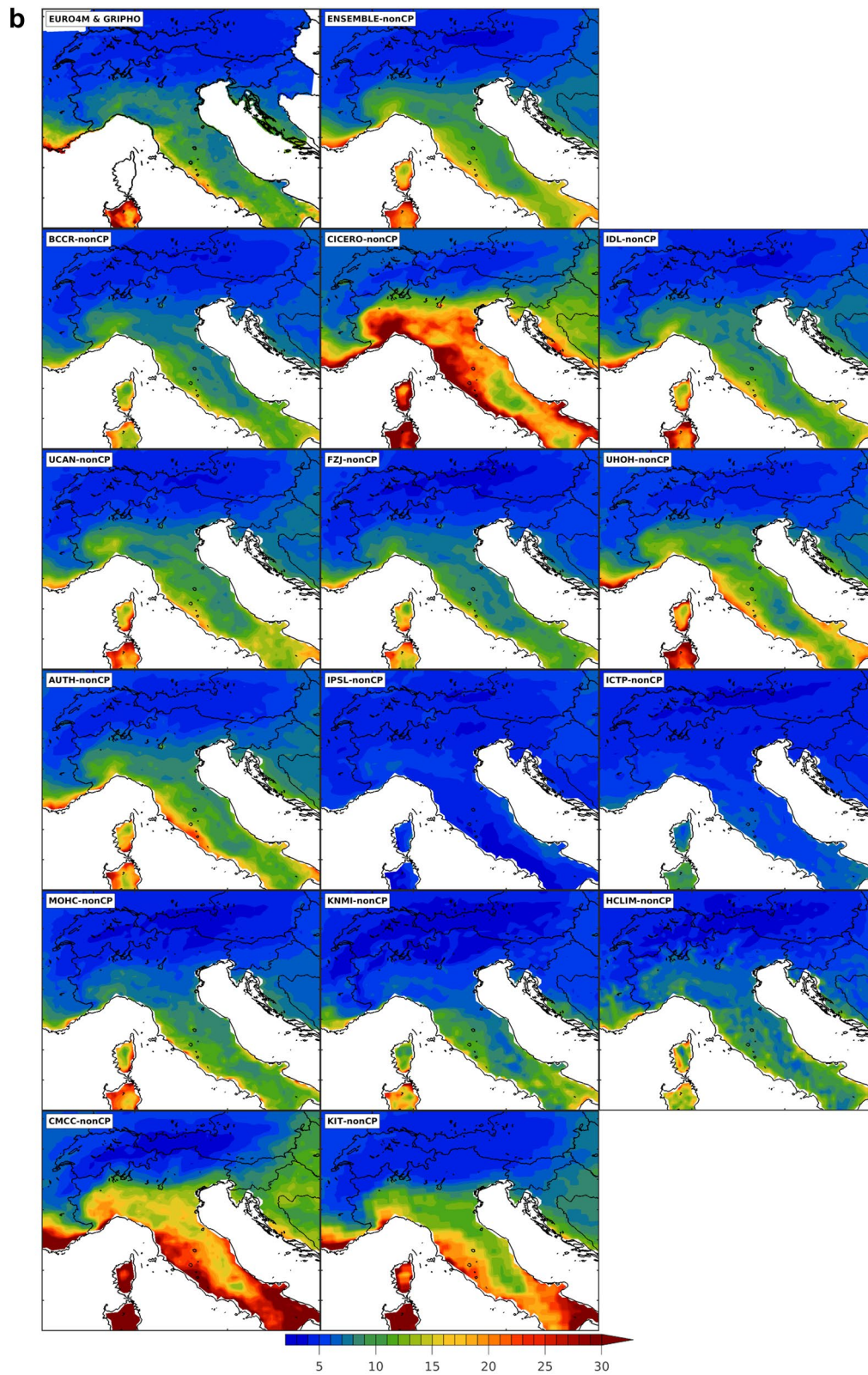


Fig. 12 (continued)

season, the 2007 initial soil moisture state does not show substantial differences between the two resolutions. A few days after, we observe a steeper soil moisture decrease in the CPRCMs ensemble, toward climatological average values, whilst the RCMs ensemble shows a smoother decrease. Both the resolutions enter dry anomaly in the second half of June. Also in this case, differences in soil moisture fade during the long-standing dry period during a large part of July and the first half of August. At the turn of mid-August, higher RCMs ensemble soil moisture is established combined with several larger precipitation events in the RCMs ensemble compared to the CPRCMs ensemble.

Finally, similarly in the two summer seasons analyzed the largest Tmax modulation is not synchronized with the occurrences of HWs but rather mainly determined by different soil moisture levels driven in turn by the different precipitation events intensity/frequency characterizing the two resolutions. Moreover, different heat fluxes partitioning can elucidate temperature differences in the two resolutions, and similarly in the two resolutions, HWs occurrence does not match with sensible heat peaks. This latter fact highlights non-local-scale advective forcing contributing to the onset of HWs in both CPRCMs and RCMs.

4 Discussions and Conclusion

In recent years, several studies investigated historical period performance and projected climate change signal generated by the latest generation of very high-resolution (km-scale or convection-permitting scale) climate models. These studies have been largely focused on precipitation (Kendon et al. 2012, 2016; Ban et al. 2015, 2021; Fosser et al. 2017; Berthou et al. 2018; Coppola et al. 2020; Knist et al. 2018; Vanden Broucke et al. 2019; Lenderink et al. 2019; Pichelli et al. 2021; Adinolfi et al. 2021). Feedbacks from a km-scale representation of land–atmosphere interactions on the temperature are still largely unexplored (Knist et al. 2020; Soares et al. 2022).

This present study explores whether and why km-scale modeling modulates HWs and local-scale forcing processes representation, taking advantage of a multimodel ensemble from CORDEX-FPS Convection initiative. In this regard, past studies highlight soil moisture–precipitation feedback modifications (Pielke 2001; Koster et al. 2004), up to the sign change in wet–arid transitional areas, when moving from a parameterized to an explicit treatment of deep–convection processes (Hohenegger et al. 2009; Taylor et al. 2013). A different soil moisture–precipitation feedback impacts the heat flux partitioning, which can in turn consistently affect temperature, in particular, summer extremes.

We summarize the main results as follows:

- Regarding the temperature, our results show warmer conditions during HWs, and generally in the summer season, in CPRCMs compared to the driving RCMs. From a multi-model perspective, km-scale modulation toward warmer–drier conditions seems to be more scale-dependent than model-dependent. This modification is generally observed in all models (except one) although with substantial inter-model spread. Considering 2003, 2006, and 2007 HWs the CPRCMs ensemble shows higher temperature than the corresponding RCMs ensemble of about 1 °C and 1.5 °C over Po valley and Adriatic regions respectively. IPSL, ICTP, MOHC, and KNMI (this latter only over Po valley) models show the largest HWs temperature modulation, exceeding in some cases 3 °C. Other HW metrics like HWMId, timing, and persistence do not show substantial differences between the two resolutions.
- Considering gridded reference products, CPRCMs' warmer signal represents a reduction of cold biases and at the same time an exacerbation of warm biases generated by the RCMs. This latter result is especially evident over the flat terrain of the Po valley. Similarly, CPRCMs temperatures are higher over the Alps and Adriatic domains but correspond to smaller biases. However, considering JJA Tmax, a distribution-based local-scale evaluation shows an ensemble mean added value of CPRCMs compared to the driving RCMs (positive DAV) over the 69% of reference sites which increases to 95% when only the distribution right tail is considered. This suggests that the CPRCMs warmer/drier tendency is likely more realistic and more accurate than the RCMs.
- Behind temperature modulation, we found lower (higher) latent (sensible) heat fluxes in the CPRCMs. In this regard, CPRCMs present drier conditions than the corresponding RCMs (excluding the CMCC model). This feature results in all the three domains (up to -25% considering ensemble mean) and not only during HWs but in general during the summer months. The different heat fluxes partitioning corresponds to a stronger land–atmosphere coupling in CPRCMs, characterized by higher Bowen ratio and lower evaporative fraction. A distinct annual cycle of soil moisture differences, with a sharp increase of differences during summer months, suggests that the CP-scale signal albeit not limited to the summer season is most prominent during the warm semester.
- Drier conditions are combined to consistently longer DSL in the CPRCMs ensemble. A doubling of CPRCMs DSL with respect to RCMs results over flat terrains and coastal areas. Compared to the observations, this km-scale DSL extension corresponds to a dry bias, especially over the Po valley subdomain. A substantial reduction of precipitation frequency especially in the summer season and continental plains agrees with other studies involving

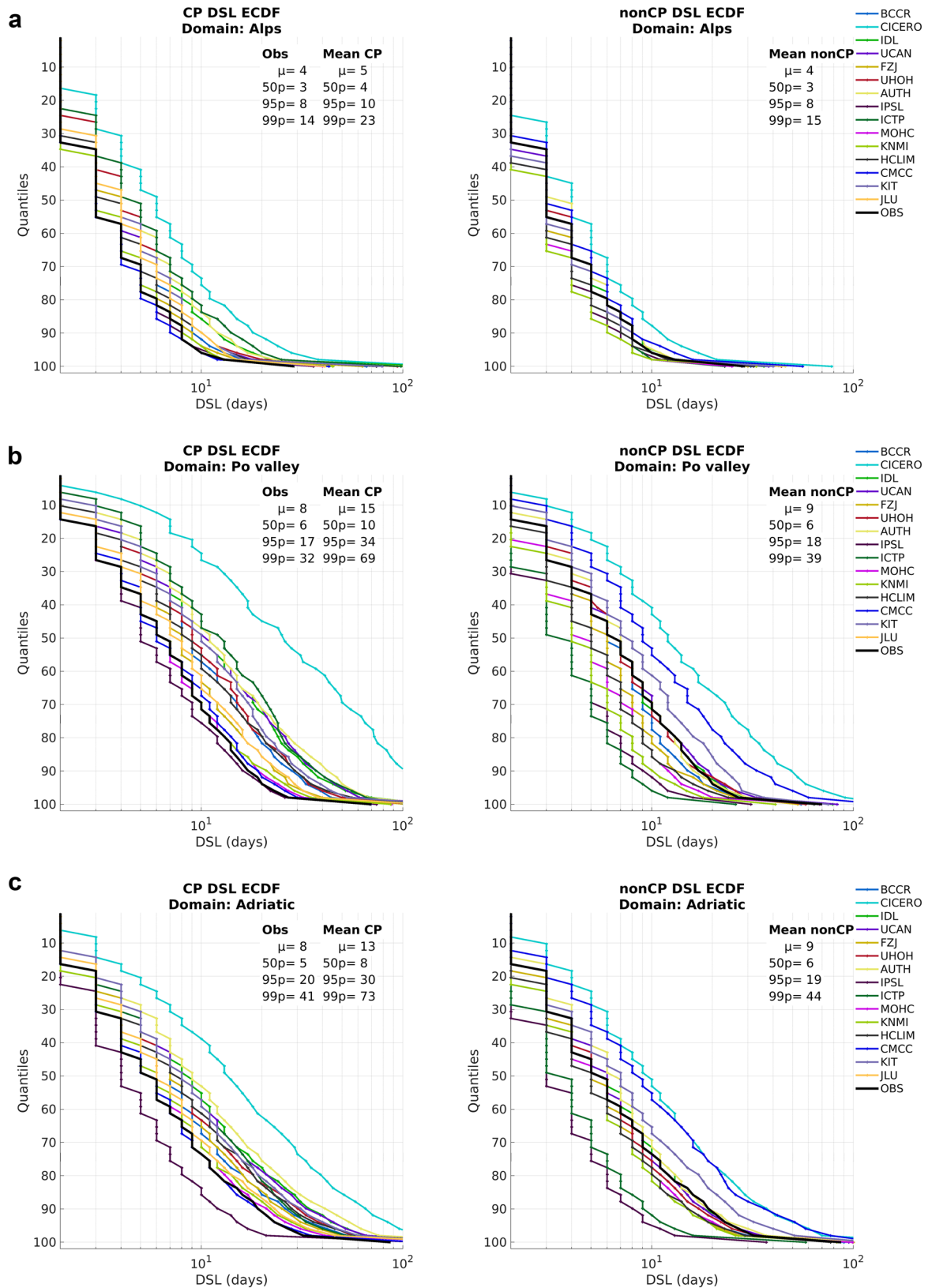


Fig. 13 Grid-node specific DSL empirical cumulative distribution functions (ECDFs) for CPRCMs (left panels), RCMs (right panels), and reference products (EURO4M for the Alpine and Po valley domains, GRIPHO dataset for the Adriatic domain). The ECDFs are built considering the 2000–2009 summer season daily precipitation time series from each grid node with no interpolation performed. The main statistics (mean, median, 95th, and 99th percentile) of the observed and simulated DSL are shown in the upper part of each panel. Results are shown for the three subdomains: Alps (a), Po valley (b), and Adriatic (c)

different areas and different models (Kendon et al. 2016, 2019; Berthou et al. 2018; Barlage et al. 2021; Ha et al. 2022).

It is difficult to disentangle interacting mechanisms driving km-scale modulation. Some insights can be retrieved considering the two models showing the largest temperature modulation (ICTP and MOHC). MOHC model shows larger modulation of soil moisture with respect to the ICTP model considering both 2003 HW (Fig. 9a, b) and summer seasons of the whole evaluation period (Fig. SM 9a and SM 9b). Differently, the ICTP model shows a larger modification of DSL than the MOHC model (Fig. 12a, b).

In the case of the MOHC model, arguments can be made over a larger role played by a different configuration of the land surface model in determining the alteration of land–atmosphere interactions between the two resolutions. In this regard, Berthou et al. (2020) show that CP-scale simulations are affected by an excess of water disappearing from the land surface through runoff whereas draining to the second soil layer at lower resolution determines substantial differences in surface soil moisture levels.

Differently from MOHC, the ICTP model presents the same land surface model configuration in the two resolutions. Here, a relevant role could be played by different PBL and cloud microphysics schemes, resulting in different sensitivity to the convection triggering processes in the two resolutions. Further, the entrainment of environmental drier air in convective plumes is parameterized in RCMs, which may partially explain the spread between models. In CPRCMs, the mixing is explicit, and this affects the triggering of precipitation (and also dissipative effects). In a related research Ha et al. (2022) have demonstrated that for similar tropospheric temperature ranges, the convection triggering is suppressed in CPRCMs. More in detail, CPRCMs are characterized by a higher integrated water vapor critical value that must be reached to trigger precipitation, combined with a lower probability of exceeding this critical value. This latter is another factor explaining the differences between RCMs and CPRCMs DSL. The relevance of the microphysics scheme choice is also evident, considering the differences between WRF IPSL and UHOH; models sharing the same

physics schemes combination except for the microphysics scheme.

It is relevant remarking that these two modulations (soil moisture and DSL) cannot be considered different/independent processes. PBL state strongly depends on the land surface processes representation whose impact is not constrained to the lower PBL but extends up to the interfacial layer and the lower troposphere mixing processes (e.g., Milovac et al. 2016). This can also be observed in Fig. 14, where a higher PBL limit can be observed in CPRCMs ensemble during both HW and non-HW conditions and mostly following differences in soil moisture. In any case, the results of the present study are not sufficient to elucidate which part of the warmth/dryness in CPRCMs can be ascribed to land–atmosphere coupling and/or "atmospheric only" processes.

Nevertheless, soil moisture constitutes a key variable for temperature extremes and different aspects can contribute to its alteration when moving to a km-scale. In this context robust evidence pertains to the modified summer convective precipitation diurnal cycle resulting in less frequent and more intense events, explored in recent studies (Berthou et al. 2020; Kendon et al. 2019; Prein et al. 2021). At the same time, large uncertainty affects the representation of soil moisture–precipitation feedback, which still remains a challenge (e.g., Yang et al. 2018; Kendon et al. 2020; Leutwyler et al. 2021). The lower part of this feedback loop (i.e., soil and land-surface processes) is parameterized by the land-surface models, which are typically developed offline and coupled to the atmospheric part of weather and climate models. With an increase in the horizontal resolution, these models are becoming more complex with more parameterized sub-grid scale processes, and they start to play a significant role, especially in representing land surface–atmosphere feedbacks which have been recognized as a large source of uncertainty (Kendon et al. 2020). In this regard, recent studies point out the relevance of explicitly representing land surface/subsurface processes when approaching km-scale climate modeling (Graf et al. 2021; Folwell et al. 2022; Guion et al. 2022; Polcher et al. 2022; Warrach-Sagi et al. 2022). Amongst others, vegetation dynamics, surface moisture heterogeneity, gradients between moisture convergence and divergence zones, and connection of groundwater to the land surface are crucial for the development and self-amplification of dry-hot extremes feedbacking with the atmosphere through differentiating evapotranspiration (Shrestha et al. 2015; Furusho-Percot et al. 2022). However, those processes are still quite crudely represented in the current km-scale simulations land models, and relative misrepresentation may have different impacts at different resolutions. At the same time, this could contribute to generate a common km-scale signature in almost all

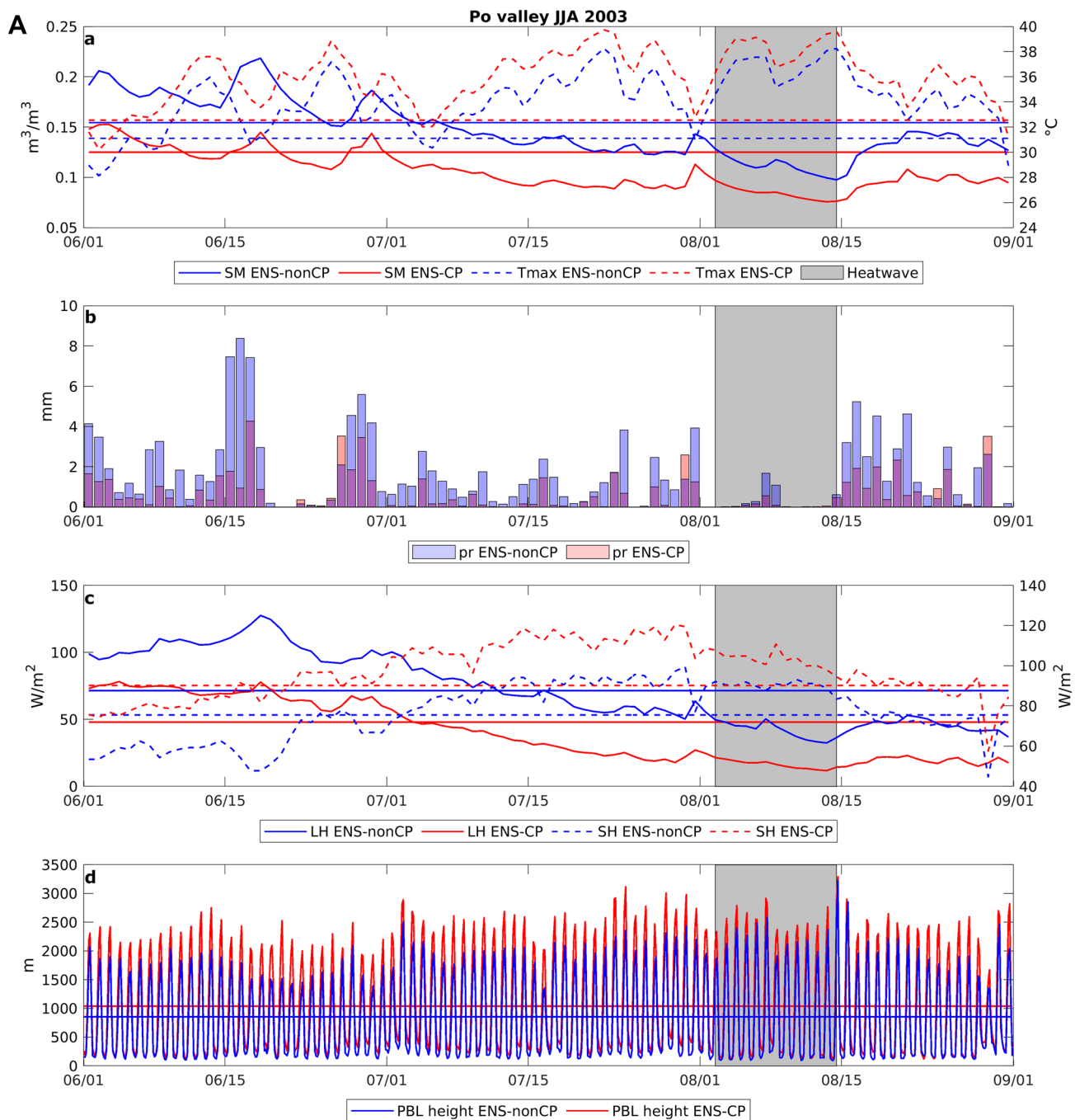


Fig. 14 Ensemble mean time series of a set of variables related to HWs and surface processes, spatially averaged for a regional box corresponding to the Po Valley subdomain. 2003 and 2007 summer seasons along with related most intense HW events are shown in (a, b) respectively. For each one, subplots (a) show daily soil top layer soil moisture (solid lines) and Tmax (dashed lines). Subplots (b)

daily mean precipitation. Subplots (c) latent (solid lines) and sensible (dashed lines) heat fluxes. Subplots (d) PBL height. All the variables have a daily mean temporal aggregation except for the PBL height reported at three-hourly temporal aggregation. Horizontal lines represent climatological mean values derived over the entire evaluation period (2000–2009 summer seasons)

models. A good example is represented by the increasingly relevant inclusion of groundwater when a resolution lower than 3 km is considered. Groundwater can represent an additional water source critical to replenish

upper layers soil moisture and is identified as an effective pathway to mitigate warm summer season biases thanks to increased evapotranspiration (Barlage et al. 2021). With the increase in spatial resolution, the role of the accurate

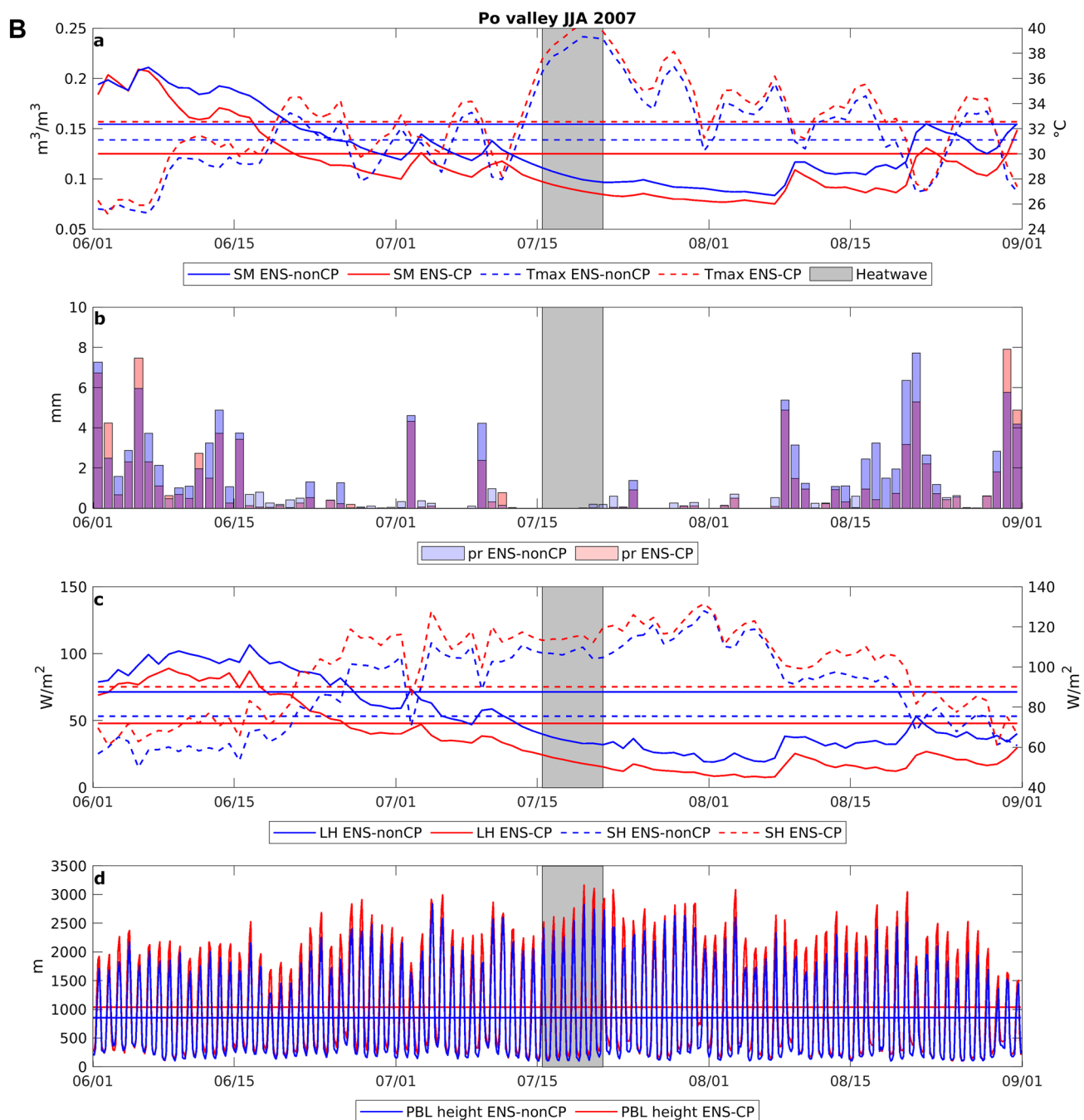


Fig. 14 (continued)

representation of these feedbacks is becoming crucial, especially considering cumulative effects in climate time scales (e.g., Seneviratne et al. 2010). In fact, in the next decades, vast continental areas are projected to shift toward wet-dry transitional conditions, characterized by a strong land-atmosphere coupling, where atmospheric variables are largely constrained by soil conditions (Knist et al. 2017; Careto et al. 2018; Soares et al. 2019).

In this study we presented the first km-scale ensemble-based summer season maximum temperature analysis, highlighting that km-scale effects go beyond the well-documented modifications of precipitation extremes introducing a modification of summer maximum temperature and HW events.

A local-scale evaluation of summer maximum temperature suggests the warmer/drier signal moving to a km-scale is likely more realistic and more accurate than the RCMs.

It is in any case not possible to fully disentangle the role of resolution increase vs. the role of improved physics which are inextricably linked. Further process-based studies are needed to confirm that these modifications are physically plausible signaling an improvement. Particular attention is recommended on summer convection inhibition at km-scale and on to disentangle the role of different mechanisms underlying km-scale modification, e.g., soil moisture-precipitation feedbacks but also the PBL, shallow convection, and microphysical parameterization schemes. These aspects can be of particular relevance considering cumulative effects on multi-decadal climate temporal scales and future projections. In this context, the next research will focus on the potential implications of evaluation experiment findings on HWs' future changes, exploring if future changes in soil moisture will show a resolution dependency and if the km-scale warmer-drier signature can be expected time-stationary or amplified/reduced in a future warmer climate.

Supplementary Information The online version contains supplementary material available at <https://doi.org/10.1007/s00382-023-06769-9>.

Acknowledgements All authors gratefully acknowledge the WCRP-CORDEX-FPS on Convective phenomena at high resolution over Europe and the Mediterranean and the research data exchange infrastructure and services provided by the Jülich Supercomputing Centre, Germany, as part of the Helmholtz Data Federation initiative. EK and SK acknowledge that this work was supported by computational time granted from the National Infrastructures for Research and Technology S.A. (GRNET S.A.) in the National HPC facility—ARIS—under project ID pr009020_thin. RMC and PMMS were supported by project LEADING – PTDC/CTA-MET/28914/2017, and project UIDB/50019/2020—IDL. JM acknowledges the support of the funding from the Spanish Agencia Estatal de Investigación through the Unidad de Excelencia Mar'ía de Maeztu with reference MDM-2017-0765. JF and SS acknowledge support from the Spanish Agencia Estatal de Investigación (MCIN/AEI/0.13039/501100011033) through project CORDyS (PID2020-116595RB-I00). UCAN simulations were carried out on the Altamira Supercomputer at the Institute of Physics of Cantabria (IFCA-CSIC), member of the Spanish Supercomputing Network. ØH acknowledges funding from the Research Council of Norway (grant no. 275589, GREAT project) and computing resources from Notur (NN9188K). LS acknowledges funding from PON Ricerca e Innovazione 2014–2020 “AIM”—Attraction and international mobility program. EU Social Fund and Regional Development Fund; Ministero dell'Istruzione e della Ricerca, grant number AIM1858058. Computing resources at CETEMPS (University of L'Aquila) and from The Norwegian academic high-performance computing and storage services Notur/Norstore projects NN9280K/NS9001K. Finally, LS thanks Maria Chara Karypidou (AUTH) for the helpful discussions about part of the study results. DB acknowledges the EU Horizon 2020 project EUCP (Grant no. 776613) and the Formas EDUCAS project (grant no. 2019-00829).

Data availability The datasets analyzed in the current study are not publicly available but will be published in the near future.

Open Access This article is licensed under a Creative Commons Attribution 4.0 International License, which permits use, sharing, adaptation, distribution and reproduction in any medium or format, as long

as you give appropriate credit to the original author(s) and the source, provide a link to the Creative Commons licence, and indicate if changes were made. The images or other third party material in this article are included in the article's Creative Commons licence, unless indicated otherwise in a credit line to the material. If material is not included in the article's Creative Commons licence and your intended use is not permitted by statutory regulation or exceeds the permitted use, you will need to obtain permission directly from the copyright holder. To view a copy of this licence, visit <http://creativecommons.org/licenses/by/4.0/>.

References

- Adinolfi M, Raffa M, Reder A, Reder A (2021) Evaluation and expected changes of summer precipitation at convection permitting scale with COSMO-CLM over Alpine Space. *Atmosphere* 2020 12:54. <https://doi.org/10.3390/atmos12010054>
- Ban N, Schmidli J, Schär C (2015) Heavy precipitation in a changing climate: does short-term summer precipitation increase faster? *Geophys Res Lett* 42:1165–1172. <https://doi.org/10.1002/2014GL062588>
- Ban N, Caillaud C, Coppola E et al (2021) The first multi-model ensemble of regional climate simulations at kilometer-scale resolution, part I : evaluation of precipitation. *Clim Dyn*. <https://doi.org/10.1007/s00382-021-05708-w>
- Barlage M, Chen F, Rasmussen R et al (2021) The Importance of scale-dependent groundwater processes in land-atmosphere interactions over the Central United States. *Geophys Res Lett* 48:1–10. <https://doi.org/10.1029/2020GL092171>
- Bauer-Marschallinger B, Stachl T (2019) Copernicus Global Land Operations “Vegetation and Energy” “CGLOPS-1” https://land.copernicus.eu/global/sites/cgls.vito.be/files/products/CGLOPS1_SQE2018_SWIV3_I1.00.pdf
- Bazile E, Abida R, Verelle A, Le Moigne P, Szczypka C (2017) MESCAN-SURFEX Surface Analysis. Deliverable D2.8 of the UERRA Project. Available online: <http://www.uerra.eu/publications/deliverable-reports.html>. Accessed 10 May 2021
- Berthou S, Kendon EJ, Chan SC et al (2020) Pan-European climate at convection-permitting scale: a model intercomparison study. *Clim Dyn* 55:35–59. <https://doi.org/10.1007/s00382-018-4114-6>
- Black E, Blackburn M, Harrison G et al (2004) Factors contributing to the summer 2003 European heatwave. *Weather* 59:217–223. <https://doi.org/10.1256/wea.74.04>
- Careto JAM, Cardoso RM, Soares PMM, Trigo RM (2018) Land-atmosphere coupling in CORDEX-Africa: hindcast regional climate simulations. *J Geophys Res Atmos* 123:11048–11067. <https://doi.org/10.1029/2018JD028378>
- Careto JAM, Soares PMM, Cardoso RM et al (2022) Added value of EURO-CORDEX high-resolution downscaling over the Iberian Peninsula revisited—part 2: max and min temperature. *Geosci Model Dev* 15:2635–2652. <https://doi.org/10.5194/gmd-15-2635-2022>
- Cioni G, Hohenegger C (2017) Effect of soil moisture on diurnal convection and precipitation in large-eddy simulations. *J Hydrometeorol* 18:1885–1903. <https://doi.org/10.1175/JHM-D-16-0241.1>
- Coppola E, Sobolowski S, Pichelli E et al (2020) A first-of-its-kind multi-model convection permitting ensemble for investigating convective phenomena over Europe and the Mediterranean. *Clim Dyn* 55:3–34. <https://doi.org/10.1007/s00382-018-4521-8>
- Dee DP, Uppala SM, Simmons a. J, et al (2011) The ERA-Interim reanalysis: Configuration and performance of the data assimilation system. *Q J R Meteorol Soc* 137:553–597. <https://doi.org/10.1002/qj.828>

- Déqué M, Jones RG, Wild M et al (2005) Global high resolution versus Limited Area Model climate change projections over Europe: quantifying confidence level from PRUDENCE results. *Clim Dyn* 25:653–670. <https://doi.org/10.1007/s00382-005-0052-1>
- Dole R, Hoerling M, Perlwitz J et al (2011) Was there a basis for anticipating the 2010 Russian heat wave? *Geophys Res Lett* 38:1–5. <https://doi.org/10.1029/2010GL046582>
- Fantini A (2019) Climate change impact on flood hazard over Italy. Ph.D. thesis, Università degli Studi di Trieste. <http://hdl.handle.net/11368/2940009>
- Feudale L, Shukla J (2007) Role of Mediterranean SST in enhancing the European heat wave of summer 2003. *Geophys Res Lett* 34:2–5. <https://doi.org/10.1029/2006GL027991>
- Findell KL, Eltahir EAB (2003) Atmospheric controls on soil moisture-boundary layer interactions. Part I: Framework development. *J Hydrometeorol* 4:552–569. [https://doi.org/10.1175/1525-7541\(2003\)004](https://doi.org/10.1175/1525-7541(2003)004)
- Fischer EM, Schär C (2010) Consistent geographical patterns of changes in high-impact European heatwaves. *Nat Geosci* 3:398–403. <https://doi.org/10.1038/ngeo866>
- Fischer EM, Seneviratne SI, Vidale PL et al (2007) Soil moisture-atmosphere interactions during the 2003 European summer heat wave. *J Clim* 20:5081–5099. <https://doi.org/10.1175/JCLI4288.1>
- Folwell SS, Taylor CM, Stratton RA (2022) Contrasting contributions of surface hydrological pathways in convection permitting and parameterised climate simulations over Africa and their feedbacks on the atmosphere. *Clim Dyn* 59:633–648. <https://doi.org/10.1007/s00382-022-06144-0>
- Fosser G, Khodayar S, Berg P (2017) Climate change in the next 30 years: what can a convection-permitting model tell us that we did not already know? *Clim Dyn* 48:1987–2003. <https://doi.org/10.1007/s00382-016-3186-4>
- Furusho-Percot C, Goergen K, Hartick C et al (2022) Groundwater model impacts multiannual simulations of heat waves. *Geophys Res Lett*. <https://doi.org/10.1029/2021GL096781>
- Giorgi F, Jones C, Asrar GR (2009) Addressing climate information needs at the regional level : the CORDEX framework. *WMO Bull* 58:175–183
- Graf M, Arnault J, Fersch B, Kunstmann H (2021) Is the soil moisture precipitation feedback enhanced by heterogeneity and dry soils? A comparative study. *Hydrol Process*. <https://doi.org/10.1002/hyp.14332>
- Guion A, Turquety S, Polcher J et al (2022) Droughts and heatwaves in the Western Mediterranean : impact on vegetation and wildfires using the coupled WRF-ORCHIDEE regional model (RegIPSL). *Clim Dyn* 58:2881–2903. <https://doi.org/10.1007/s00382-021-05938-y>
- Ha MT, Bastin S, Drobinski P et al (2022) Precipitation frequency in Med-CORDEX and EURO-CORDEX ensembles from 0.44 ° to convection-permitting resolution : impact of model resolution and convection representation. *Clim Dyn*. <https://doi.org/10.1007/s00382-022-06594-6>
- Halladay K, Berthou S, Kendon E (2021) Understanding differences in land-atmosphere interactions between pan-European convection-permitting and parameterised climate models. *EGU Gen Assembly Conf Abs pp*. EGU21-14859. <https://doi.org/10.5194/egusphere-egu21-14859>
- Haylock MR, Hofstra N, Tank K, a. MG, et al (2008) A European daily high-resolution gridded data set of surface temperature and precipitation for 1950–2006. *J Geophys Res Atmos*. <https://doi.org/10.1029/2008JD010201>
- Hodnebrog O, Marelle L, Alterskjær K et al (2019) Intensification of summer precipitation with shorter time-scales in Europe. *Environ Res Lett*. <https://doi.org/10.1088/1748-9326/ab549c>
- Hohenegger C, Brockhaus P, Bretherton CS, Schär C (2009) The soil moisture-precipitation feedback in simulations with explicit and parameterized convection. *J Clim* 22:5003–5020. <https://doi.org/10.1175/2009JCLI2604.1>
- Hong JS, Yeh SW, Seo KH (2018) Diagnosing physical mechanisms leading to pure heat waves versus pure tropical nights over the Korean Peninsula. *J Geophys Res Atmos* 123:7149–7160. <https://doi.org/10.1029/2018JD028360>
- Horton DE, Johnson NC, Singh D et al (2015) Contribution of changes in atmospheric circulation patterns to extreme temperature trends. *Nature* 522:465–469. <https://doi.org/10.1038/nature14550>
- Imamovic A, Schlemmer L, Schär C (2017) Collective impacts of orography and soil moisture on the soil moisture-precipitation feedback. *Geophys Res Lett* 44(22):11,682–11,691. <https://doi.org/10.1002/2017GL075657>
- Isotta FA, Frei C, Weigluni V et al (2014) The climate of daily precipitation in the Alps: Development and analysis of a high-resolution grid dataset from pan-Alpine rain-gauge data. *Int J Climatol* 34:1657–1675. <https://doi.org/10.1002/joc.3794>
- Jiang A, Liu X, Czarnecki E, Zhang C (2019) Hourly weather data projection due to climate change for impact assessment on building and infrastructure. *Sustain Cities Soc* 50:101688. <https://doi.org/10.1016/j.scs.2019.101688>
- Kendon EJ, Roberts NM, Senior CA, Roberts MJ (2012) Realism of rainfall in a very high-resolution regional climate model. *J Clim* 25:5791–5806. <https://doi.org/10.1175/JCLI-D-11-00562.1>
- Kendon EJ, Ban N, Roberts NM et al (2016) Do convection-permitting regional climate models improve projections of future precipitation change? *Bull Am Meteorol Soc* 98:79–93. <https://doi.org/10.1175/bams-d-15-0004.1>
- Kendon EJ, Stratton RA, Tucker S et al (2019) Enhanced future changes in wet and dry extremes over Africa at convection-permitting scale. *Nat Commun*. <https://doi.org/10.1038/s41467-019-09776-9>
- Kendon EJ, Prein AF, Senior CA et al (2020) Challenges and outlook for convection-permitting climate modelling. *Philos Trans R Soc*. <https://doi.org/10.1098/rsta.2019.0547>
- Klein Tank AMG, Wijngaard JB, Können GP et al (2002) Daily dataset of 20th-century surface air temperature and precipitation series for the European Climate Assessment. *Int J Climatol* 22:1441–1453. <https://doi.org/10.1002/joc.773>
- Knist S, Goergen K, Buonomo E et al (2017) Land-atmosphere coupling in EURO-CORDEX evaluation experiments. *J Geophys Res* 122:79–103. <https://doi.org/10.1002/2016JD025476>
- Knist S, Goergen K, Simmer C (2018) Evaluation and projected changes of precipitation statistics in convection-permitting WRF climate simulations over Central Europe. *Clim Dyn*. <https://doi.org/10.1007/s00382-018-4147-x>
- Knist S, Goergen K, Simmer C (2020) Effects of land surface inhomogeneity on convection-permitting WRF simulations over central Europe. *Meteorol Atmos Phys* 132:53–69. <https://doi.org/10.1007/s00703-019-00671-y>
- Kornhuber K, Osprey S, Coumou D et al (2019) Extreme weather events in early summer 2018 connected by a recurrent hemispheric wave-7 pattern. *Environ Res Lett*. <https://doi.org/10.1088/1748-9326/ab13bf>
- Koster RD, Dirmeyer PA, Guo Z et al (2004) Regions of strong coupling between soil moisture and precipitation. *Science* (80-) 305:1138–1140. <https://doi.org/10.1126/science.1100217>
- Koster RD, Schubert SD, Suarez MJ (2009) Analyzing the concurrence of meteorological droughts and warm periods, with implications for the determination of evaporative regime. *J Clim* 22:3331–3341. <https://doi.org/10.1175/2008JCLI2718.1>
- Lenderink G, Belušić D, Fowler HJ et al (2019) Systematic increases in the thermodynamic response of hourly precipitation extremes in an idealized warming experiment with a convection-permitting

- climate model. *Environ Res Lett*. <https://doi.org/10.1088/1748-9326/ab214a>
- Leutwyler D, Imamovic A, Schär C (2021) The continental-scale soil moisture-precipitation feedback in Europe with parameterized and explicit convection. *J Clim* 34:5303–5320. <https://doi.org/10.1175/JCLI-D-20-0415.1>
- Milovac J, Warrach-Sagi K, Behrendt A, Späth F, Ingwersen J, Wulfmeyer V (2016) Investigation of PBL schemes combining the WRF model simulations with scanning water vapor differential absorption lidar measurements. *J Geophys Res Atmos* 121:624–649. <https://doi.org/10.1002/2015JD023927>
- Miralles DG, Van Den Berg MJ, Teuling AJ, De Jeu RAM (2012) Soil moisture-temperature coupling: a multiscale observational analysis. *Geophys Res Lett* 39:2–7. <https://doi.org/10.1029/2012GL053703>
- Miralles DG, Teuling AJ, Van Heerwaarden CC, De Arellano JVG (2014) Mega-heatwave temperatures due to combined soil desiccation and atmospheric heat accumulation. *Nat Geosci* 7:345–349. <https://doi.org/10.1038/ngeo2141>
- Miralles DG, Gentile P, Seneviratne SI, Teuling AJ (2019) Land-atmospheric feedbacks during droughts and heatwaves: state of the science and current challenges. *Ann N Y Acad Sci* 1436:19–35. <https://doi.org/10.1111/nyas.13912>
- Molina MO, Sánchez E, Gutiérrez C (2020) Future heat waves over the Mediterranean from an Euro-CORDEX regional climate model ensemble. *Sci Rep* 10(1):1–10. <https://doi.org/10.1038/s41598-020-65663-0>
- Muñoz-Sabater J, Dutra E, Agustí-Panareda A et al (2021) ERA5-Land: a state-of-the-art global reanalysis dataset for land applications. *Earth Syst Sci Data Discuss*. <https://doi.org/10.5194/essd-2021-82>
- Myhre G, Samset BH, Hodnebrog O et al (2018) Sensible heat has significantly affected the global hydrological cycle over the historical period. *Nat Commun*. <https://doi.org/10.1038/s41467-018-04307-4>
- Naz BS, Kollet S, Franssen HJH et al (2020) A 3 km spatially and temporally consistent European daily soil moisture reanalysis from 2000 to 2015. *Sci Data* 7:111. <https://doi.org/10.1038/s41597-020-0450-6>
- Perkins SE (2015) A review on the scientific understanding of heatwaves—Their measurement, driving mechanisms, and changes at the global scale. *Atmos Res* 164–165:242–267. <https://doi.org/10.1016/j.atmosres.2015.05.014>
- Perkins SE, Alexander LV (2013) On the measurement of heat waves. *J Clim* 26:4500–4517. <https://doi.org/10.1175/JCLI-D-12-00383.1>
- Perkins SE, Pitman AJ, Holbrook NJ, McAneney J (2007) Evaluation of the AR4 climate models' simulated daily maximum temperature, minimum temperature, and precipitation over Australia using probability density functions. *J Clim* 20:4356–4376. <https://doi.org/10.1175/JCLI4253.1>
- Perkins SE, Alexander LV, Nairn JR (2012) Increasing frequency, intensity and duration of observed global heatwaves and warm spells. *Geophys Res Lett* 39:1–5. <https://doi.org/10.1029/2012GL053361>
- Pichelli E, Coppola E, Sobolowski S et al (2021) The first multi-model ensemble of regional climate simulations at kilometer-scale resolution part 2: historical and future simulations of precipitation. *Clim Dyn*. <https://doi.org/10.1007/s00382-021-05657-4>
- Pielke RA (2001) Influence of the spatial distribution of vegetation and soils on the prediction of cumulus convective rainfall. *Rev Geophys* 39:151–177
- Polcher J, Schrapfner A, Dupont E et al (2022) Hydrological modelling on atmospheric grids; using graphs of sub-grid elements to transport energy and water. *Egusphere* [preprint]. <https://doi.org/10.5194/egusphere-2022-690>
- Prein AF, Gobiet A, Suklitsch M et al (2013) Added value of convection permitting seasonal simulations. *Clim Dyn* 41:2655–2677. <https://doi.org/10.1007/s00382-013-1744-6>
- Prein AF, Rasmussen RM, Stephens G (2017) Challenges and advances in convection-permitting climate modeling. *Bull Am Meteorol Soc*. <https://doi.org/10.1175/BAMS-D-16-0263.1>
- Prein AF, Rasmussen RM, Wang D, Giangrande SE (2021) Sensitivity of organized convective storms to model grid spacing in current and future climates. *Philos Trans R Soc A Math Phys Eng Sci*. <https://doi.org/10.1098/rsta.2019.0546>
- Ridal, M, Olsson E, Undén P, Zimmermann K, Ohlsson A (2017) Uncertainties in Ensembles of Regional Re-Analyses. Deliverable D2.7 HARMONIE Reanalysis Report of Results and Dataset. Available online: <http://www.uerra.eu/component/dpattachments/?task=attachment.download&id=296>. Accessed 10 May 2021)
- Russo S, Sillmann J, Fischer EM (2015) Top ten European heatwaves since 1950 and their occurrence in the coming decades. *Environ Res Lett*. <https://doi.org/10.1088/1748-9326/10/12/124003>
- Santanello JA, Dirmeyer PA, Ferguson CR, Findell KL, Tawfik AB, Berg A, Ek M, Gentile P, Guillod BP, Van Heerwaarden C, Roundy J, Wulfmeyer V (2018) Land-atmosphere interactions the LoCo perspective. *Bull Am Meteor Soc* 99(6):1253–1272. <https://doi.org/10.1175/BAMS-D-17-0001.1>
- Seneviratne SI, Corti T, Davin EL et al (2010) Investigating soil moisture-climate interactions in a changing climate: a review. *Earth-Sci Rev* 99:125–161. <https://doi.org/10.1016/j.earscirev.2010.02.004>
- Seneviratne SI, Koster RD (2012) A revised framework for analyzing soil moisture memory in climate data: derivation and interpretation. *J Hydrometeorol* 13:404–412. <https://doi.org/10.1175/JHM-D-11-044.1>
- Seneviratne SI, Zhang X, Adnan M et al (2021) Weather and climate extreme events in a changing climate. In: Climate change 2021: weather and climate extreme events in a changing climate. In: Masson-Delmotte V, Zhai P, Pirani A, Connors SL, Péan C, Berger S, Caud N, Chen Y, Goldfarb L, Gomis MI, Huang M, Leitzell K, Lonnoy E, Matthews JBR, Maycock TK, Waterfield T, Yelekçi O, Yu R, Zhou B (eds) Contribution of Working Group I to the SIXTH ASSESSMENT REPORT of the Intergovernmental Panel on Climate Change. Cambridge University Press (in press)
- Shrestha P, Sulis M, Simmer C, Kollet S (2015) Impacts of grid resolution on surface energy fluxes simulated with an integrated surface-groundwater flow model. *Hydrol Earth Syst Sci* 19:4317–4326. <https://doi.org/10.5194/hess-19-4317-2015>
- Soares PMM, Cardoso RM (2018) A simple method to assess the added value using high-resolution climate distributions: application to the EURO-CORDEX daily precipitation. *Int J Climatol* 38:1484–1498. <https://doi.org/10.1002/joc.5261>
- Soares PMM, Careto JAM, Cardoso RM et al (2019) Land-atmosphere coupling regimes in a future climate in Africa: from model evaluation to projections based on CORDEX-Africa. *J Geophys Res Atmos* 124:11118–11142. <https://doi.org/10.1029/2018JD029473>
- Soares PMM, Careto JAM, Cardoso RM et al (2022) The added value of km-scale simulations to describe temperature over complex orography: the CORDEX FPS-Convection multi-model ensemble runs over the Alps. *Clim Dyn*. <https://doi.org/10.1007/s00382-022-06593-7>
- Sousa PM, Barriopedro D, García-Herrera R et al (2020) Distinct influences of large-scale circulation and regional feedbacks in two exceptional 2019 European heatwaves. *Commun Earth Environ* 1:1–13. <https://doi.org/10.1038/s43247-020-00048-9>
- Taylor CM, Parker DJ, Harris PP (2007) An observational case study of mesoscale atmospheric circulations induced by soil moisture. *Geophys Res Lett* 34:2–7. <https://doi.org/10.1029/2007GL030572>

- Taylor CM, De Jeu RAM, Guichard F et al (2012) Afternoon rain more likely over drier soils. *Nature* 489:423–426. <https://doi.org/10.1038/nature11377>
- Taylor CM, Birch CE, Parker DJ et al (2013) Modeling soil moisture-precipitation feedback in the Sahel: Importance of spatial scale versus convective parameterization. *Geophys Res Lett* 40:6213–6218. <https://doi.org/10.1002/2013GL058511>
- van der Linden P, Mitchell JFB (eds) (2009). Met Office Hadley Centre, Exeter
- Vanden Broucke S, Wouters H, Demuzere M, van Lipzig NPM (2019) The influence of convection-permitting regional climate modeling on future projections of extreme precipitation: dependency on topography and timescale. *Clim Dyn* 52:5303–5324. <https://doi.org/10.1007/s00382-018-4454-2>
- Vautard R, Gobiet A, Jacob D et al (2013) The simulation of European heat waves from an ensemble of regional climate models within the EURO-CORDEX project. *Clim Dyn* 41:2555–2575. <https://doi.org/10.1007/s00382-013-1714-z>
- Warrach-Sagi K, Ingwersen J, Schwitalla T et al (2022) Noah-MP with the generic crop growth model gecros in the wrf model: effects of dynamic crop growth on land-atmosphere interaction. *J Geophys Res Atmos*. <https://doi.org/10.1029/2022JD036518>
- Wehrli K, Guillod BP (2019) Identifying key driving processes of major recent heat waves. <https://doi.org/10.1029/2019JD030635>
- Woollings T, Barriopedro D, Methven J et al (2018) Blocking and its response to climate change. *Curr Clim Chang Reports* 4:287–300. <https://doi.org/10.1007/s40641-018-0108-z>
- Wouters H, Demuzere M, Blahak U, Fortuniak K, Maiheu B, Camps J, Tieleman D, van Lipzig NPM (2016) The efficient urban canopy dependency parametrization (SURY) v1.0 for atmospheric modeling: Description and application with the COSMO-CLM model for a Belgian summer. *Geosci Model Dev* 9:3027–3054
- Yang L, Sun G, Zhi L, Zhao J (2018) Negative soil moisture-precipitation feedback in dry and wet regions. *Sci Rep* 8:1–9. <https://doi.org/10.1038/s41598-018-22394-7>
- Zhou S, Park Williams A, Berg AM et al (2019) Land–atmosphere feedbacks exacerbate concurrent soil drought and atmospheric aridity. *Proc Natl Acad Sci USA* 116:18848–18853. <https://doi.org/10.1073/pnas.1904955116>
- Zscheischler J, Westra S, Van Den Hurk BJM et al (2018) Future climate risk from compound events. *Nat Clim Chang* 8:469–477. <https://doi.org/10.1038/s41558-018-0156-3>

Publisher's Note Springer Nature remains neutral with regard to jurisdictional claims in published maps and institutional affiliations.

Authors and Affiliations

L. Sangelantoni^{1,2} · S. Sobolowski³ · T. Lorenz³ · Ø. Hodnebrog⁴ · R. M. Cardoso⁵ · P. M. M. Soares⁵ · R. Ferretti² · A. Lavín-Gullón⁶ · J. Fernandez⁶ · K. Goergen^{7,8} · J. Milovac⁶ · E. Katragkou⁹ · S. Kartsios⁹ · E. Coppola¹⁰ · E. Pichelli¹⁰ · M. Adinolfi¹¹ · P. Mercogliano¹¹ · S. Berthou¹² · H. de Vries¹³ · A. Dobler¹⁴ · D. Belušić^{15,20} · H. Feldmann¹⁶ · M. H. Tölle^{17,18} · S. Bastin¹⁹

¹ Euro-Mediterranean Center on Climate Change (CMCC), CSP division, Bologna, Italy

² CETEMPS, Department of Physical and Chemical Sciences, University of L'Aquila, L'Aquila, Italy

³ NORCE Norwegian Research Centre AS, The Bjerknes Centre for Climate Research, Bergen, Norway

⁴ Center for International Climate Research (CICERO), Oslo, Norway

⁵ Universidade de Lisboa, Faculdade de Ciências, Instituto Dom Luiz, Lisbon, Portugal

⁶ Instituto de Física de Cantabria (IFCA), CSIC-Universidad de Cantabria, Santander, Spain

⁷ Institute of Bio- and Geosciences (IBG-3, Agrosphere), Research Centre Jülich, Wilhelm-Johnen-Straße, 52428 Jülich, Germany

⁸ Centre for High-Performance Scientific Computing in Terrestrial Systems, Geoverbund ABC/J, Jülich, Germany

⁹ Department of Meteorology and Climatology, School of Geology, Aristotle University of Thessaloniki, Thessaloniki, Greece

¹⁰ International Centre for Theoretical Physics (ICTP), Trieste, Italy

¹¹ Euro-Mediterranean Center on Climate change (CMCC), REMHI division, Caserta, Italy

¹² Met Office Hadley Centre, Exeter, UK

¹³ Royal Netherlands Meteorological Institute (KNMI), De Bilt, The Netherlands

¹⁴ Norwegian Meteorological Institute, Oslo, Norway

¹⁵ Swedish Meteorological and Hydrological Institute (SMHI), Norrköping, Sweden

¹⁶ Institute of Meteorology and Climate Research (IMK-IFU), Karlsruhe Institute of Technology (KIT), Wolfgang-Gaede-Strasse 1, 76131 Karlsruhe, Germany

¹⁷ CESR (Center for Environmental Systems Research), University of Kassel, Kassel, Germany

¹⁸ Former JLU, Justus-Liebig-University Giessen, Giessen, Germany

¹⁹ Laboratoire Atmospheres Observations Spatiales (LATMOS)/Institut Pierre Simon Laplace (IPSL)/, UVSQ Université Paris-Saclay, Sorbonne Université, CNRS, Guyancourt, France

²⁰ University of Zagreb, Zagreb, Croatia